

Ainārs Knoks

PROPERTIES OF NANOSTRUCTURED TiO₂ COATING FOR DEGRADATION OF POLLUTANTS

SUMMARY OF DOCTORAL THESIS

Submitted for the degree of Doctor in the field of Physics and Astronomy Subfield: Materials Physics

The doctoral thesis was carried out in Institute of Solid state physics, University of Latvia from 2014 till 2024.



This work has been supported by the European Social Fund within the Project No 8.2.2.0/18/A/017 "Development of the academic personnel of Riga Technical University in the strategic fields of specialization".

The thesis comprises 6 chapters: introduction, literature overview, experimental setup and methodology, results and conclusions, result approbation, acknowledgments, used literature, and 1 appendix.

Form of the thesis: dissertation in the branch of Physics and Astronomy in the subbranch of Material Physics

Supervisor: Dr. phys. **Jānis Kleperis**, leading researcher at the Institute of Solid State Physics, University of Latvia.

Reviewers:

- 1) Artūrs Medvids, Dr. habil. phys., professor, Riga Technical university;
- Aivars Vembris, Dr. phys., leading researcher, Institute of Solid State Physics, University of Latvia;
- Agne Šulčiūtė, Dr. phys., Associate Professor, Kaunas University of Technology, Lithuania.

The thesis will be defended at the public session of the Doctoral Committee of Physics and Astronomy, University of Latvia, at the Institute of Solid State Physics, University of Latvia Kengaraga street 8, Riga, at 15.00 on 21st of March 2025.

The thesis is available in the Library of the University of Latvia, Kalpaka blvd. 4.

This thesis is accepted for the commencement of the degree of Doctor of Physics and Astronomy on 21st of March 2025 by the Doctoral Committee of Physics and Astronomy, and Material Science, University of Latvia.

Chaiman of the Doctoral Committee	/ Dr. habil. phys. Linards Skuja
Secretary of the Doctoral Committee	/ Sintija Siliņa ,

- © Ainārs Knoks, 2025
- © University of Latvia, 2025

ISBN 978-9934-36-352-8 ISBN 978-9934-36-353-5 (PDF)

ABSTRACT

To fulfill the ambitious global and European goals for a clean environment, smart energy, and sustainable resource management, it is essential to develop high-efficiency materials and technologies, with focus on passive systems that do not require external power. The availability and safety of critical raw materials is becoming increasingly important. As a result, efforts are being made to replace critical materials with more abundant alternatives. Currently, a significant part of catalysis-based passive and active environmental purification technologies rely on precious metals and are energy intensive. To reduce costs and increase availability alternative catalysts are needed, particularly for photocatalytic applications. This work focuses on synthesis and investigation of materials aimed at enhancing the photocatalytic properties of passive catalyst for degradation of environmental pollutants.

Titanium dioxide (TiO₂) is a known material in various industries as a food additive (E171) and a white pigment for paints, varnishes, paper, plastics, cosmetics, and others. Mainly because of titania's stability and relative harmlessness to the environment as well as human health. Considering that it is photocatalyst capable of environmental pollutant degradation, as well as water splitting, titania has the potential to facilitate solutions to some environmental pollution problems in water and air; thereby promoting sustainability, improving public health, and contributing to a cleaner future. However, TiO₂ properties and production methods must be improved to achieve these goals. Due to the wide band gap, the photocatalytic activity of TiO₂ is primarily activated by irradiation with the ultraviolet range. In addition, it has a high charge carrier recombination rate. While the synthesis method should provide a simple and scalable material without disrupting the selected set of properties. One such method is electrochemical anodization providing a large surface area due to possible nanostructuring.

In this thesis, a nanostructured TiO₂ coating was synthesized; an investigation of the coating synthesis parameters and their influence on the structure, morphology, and photocatalytic activity was done. As a result, an original two-step anodization technology for growing TiO₂ nanotubes has been developed, which involves modifying classic anodization with introduction of a low anodization voltage step, with voltages under field assisted anodization, then application of higher anodization voltage in the second step. By varying the low voltage step, it is possible to influence the resulting crystalline structure and photocatalytic properties of the coating. This modified anodization methodology allows synthesis of more active titania coatings compared to classic anodization.

To further increase the photocatalytic efficiency of the NT, a unique method for composite coating synthesis was developed, and coatings were obtained; the developed method combines the processes of anodization and electrophoresis for an *in situ* composite coating synthesis. Different additive materials were

used: WO₃, carbon nanoparticles, exfoliated graphene particles, graphene quantum dots, carbon quantum dots, and Pt doped activated carbon. The obtained results show that the additive particles affect the photocatalytic properties of the coating by changing the crystalline structure and phase composition. Using the developed method, it is possible to obtain anodic ${\rm TiO}_2$ nanotube coating with brookite phase content with improved photocatalytic properties compared to single-phase anatase or rutile ${\rm TiO}_2$ coatings.

TABLE OF CONTENTS

AB	STRACT	3
1.	GENERAL DESCRIPTION OF WORK	6
	1.1. Authors contribution	6
	1.2. Introduction	6
	1.3. Novelty	8
	1.4. Aim and Tasks of this work	9
	1.5. Defendable theses	9
	1.6. Scientific results and validation	9
	1.6.1. Reviewed Publications	10
	1.6.2. Reviewed abstracts	10
	1.6.3. Other related publications	10
	1.6.4. Participation in conferences	11
	1.7. Literature overview and background	14
2.	EXPERIMENTAL METHODS AND DESCRIPTION	19
	2.1. Determination of photoelectrochemical properties	19
	2.2. Study of structural and optical properties.	20
	2.3. Synthesis of materials and samples	22
	2.3.1. Obtaining TiO_2 NTs by electrochemical anodization	22
	2.3.2. Synthesis of Additive Carbon Materials	24
3.	RESULTS AND DISCUSSION	25
	3.1. TiO ₂ NT synthesis in an inorganic electrolyte.	25
	3.1.1. Low voltage effect on crystalline structure	28
	3.1.2. Photocatalytic properties	33
	3.1.3. Introduction of additives	34
	3.2. NT coatings synthesized in an organic electrolyte	45
	3.2.1. Effect of NT coating thickness on photophysical parameters	47
	3.2.2. Carbon particle additives in anodic coatings synthesized in an organic electrolyte	49
4.	CONCLUSIONS	55
5.	ACKNOWLEDGEMENTS	58
۶.	5.1. Projects and funding	58
	5.2. Participation in scientific projects and programs	58
6	LIST OF USED LITERATURE	60

1. GENERAL DESCRIPTION OF WORK

1.1. Authors contribution

This thesis was carried out at the Institute of Solid State Physics of the University of Latvia. All materials used in this work have been synthesized by the author, except in the case of NC and CP, elaborated further and synthesized under the author's supervision. A general summary of the parameters and modifications studied can be seen in the conclusions of this work. The estimated approximate number of syntheses is 1574. The author performed all electrochemical and catalytic properties studies (i.e., OCP, PCR, degradation coefficient determination). The author performed most of the measurements necessary for material characterization, including Raman spectroscopy, except for H, Q, and G series, which were conducted by ISSP UL colleague Jevgenij Gabrusenok, X-ray diffraction analysis (XRD), scanning electron microscopy (SEM), except CP and acquisition of NC series images by ISSP UL colleague Krišjānis Šmits, determination of optical absorption edge, Mote-Schottky measurements and analysis, determination of charge carrier concentration and flat band potential as well as processing of said data. Synthesis of additive carbon materials, H and G series. A similar adapted synthesis method was used to synthesize an exfoliated nitrogen-doped multilayer graphene (NC) series of materials under the supervision of a student, which further resulted in bachelor's and master's theses. All experimental data analysis and interpretation were performed primarily by the author in cooperation with all co-authors of scientific articles.

During the work, three bachelor's theses, two master's theses, three internships, and six high school students' scientific research works were conducted/lead, in which the author's knowledge and the developed synthesis recipes and methods for obtaining samples were used.

1.2. Introduction

One of the significant challenges Humanity faces today is environmental pollution caused by industrial activity, in addition to increasing energy demand. Thus, the necessity to eliminate the pollutants arises, such as water purification or CO_2 conversion. Although existing purification systems work well enough, these technologies heavily rely on the generated electricity, as those are energy intensive, and rare, high-cost catalysts. To reduce global energy consumption and clean up the environment, it is necessary to look for self-sufficient catalysts activated by the surrounding renewable energy resources, such as solar light. In this case, there is a need for catalysts with activity in the visible spectrum range.

Energy self-sufficient catalytic materials must embody a set of requirements to have implementation potential; one of promising photocatalysts is titanium dioxide (TiO₂), due to its stability, environmental and human health-friendly, with the ability to break down organic waste in water and exhaust gases in the atmosphere under the influence of sunlight [1; 2]. In addition, there are other applications for TiO₂, such as hydrogen energetics [3; 4], batteries [5], microbial fuel cells [6; 7], antiviral coatings, cosmetics, paints, and others.

Titanium dioxide as a catalyst is a widely investigated material – the world wide web immediately gives 8.27 million links; ${\rm TiO_2}$ is used as a food additive (E171), catalyst, pigment. 90% of more than 8 million tons produced in 2023 worldwide is used as pigment for paints, varnishes, paper and plastics, as catalysis around 10%, specifically for photocatalysis between 1 and 3%. Therefore, research continues, and significant work by the scientific community has been devoted to modified ${\rm TiO_2}$ catalysts with dopants such as Au, Ag, Pt, Pd, S, C, or additives WO₃, carbon quantum dots, CdS, Al₂O₃, and others.

Although various methods can obtain TiO₂, the synthesis methodology used to achieve the set goal must coincide with selected parameters and provide a large surface area with potential scalability. These conditions are primarily fulfilled by the electrochemical anodization method. However, a couple of disadvantages of this method have been observed, e.g., a substantial number of research teams use very harmful substances like HF, sometimes even at elevated temperatures [8]. This means that it is necessary to look for ways to replace this substance while maintaining the positive possibilities of the method. In the reviewed literature, it was also observed that the methods of introducing additives are both complex and energy-intensive, in addition to somewhat limited scalability.

One of the advantages of anodic TiO_2 is the ability to modify its morphology according to the chosen application; in this work, synthesis of the self-oriented nanotube (NT) coatings with a large active surface area, which is essential for a catalyst, was done and optimization of photocatalytic properties was carried out. The position of the conduction band (CB) lower level and valence band (VB) upper level of TiO_2 in relation to the reduction-oxidation (*red-ox*) potentials of

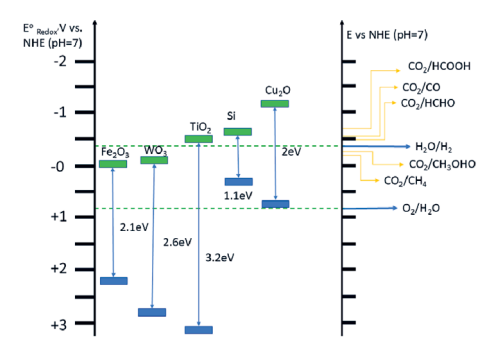


Fig. 1. Comparison of photocatalyst band gap edge potentials compared to water, \mathbf{CO}_2 , and other molecule red-ox potential, adapted from [9; 10]

water and other organic molecules allows a sufficient potential of photogenerated electron-hole (e⁻-h⁺) pairs to be able to degrade various environmental pollutants. An example from the location of ox-red potentials is given Fig. 1.

There is a knowledge gap in relation of the growth mechanism of ${\rm TiO_2}$ nanotubes (NT) under certain synthesis conditions, such as low voltage application, and its effect on their structural and photophysical properties. This has yet to be studied. Furthermore, despite many doping and additive materials, and techniques in an effort to improve the photocatalytic properties of ${\rm TiO_2}$ for various applications; there is virtually no information on in situ techniques of additive introduction during anodization. Existing technologies involve complex, resource-intensive methods, and additives rarely change the obtained crystalline phase composition in ${\rm TiO_2}$ materials.

1.3. Novelty

An efficient and durable photocatalyst is needed to ensure effective and sustainable photocatalytic pollution treatment. In addition, customization of the material required for functionality should be accessible and straightforward. To obtain anodic ${\rm TiO_2}$, especially in an inorganic electrolyte, hydrofluoric acid and a long anodization time, usually measured in several hours, are often used. In addition to increase the photocatalytic activity via modifications introduced are performed by resource-intensive methods such as ion implantation [11], precious metal thin film coatings [8] etc.

In the framework of this thesis, a modified anodization method was developed to obtain coatings with increased catalytic properties in an inorganic electrolyte. The main contribution of this unique method is to divide the anodization into two steps without interrupting the anodization process or changing the electrolyte. The first step is the low voltage step, which provides a low voltage for a certain period of time, with voltage value that does not allow field assisted nanostructuring. The second is the anodization step, which uses a higher anodization voltage above the said threshold of nanostructuring. Introducing the first step promotes the proportion of the anatase phase in the obtained samples, thus increasing the photocatalytic properties and promotes the formation of TiO_2 NTs.

In addition, a unique combined method of obtaining nanostructured ${\rm TiO_2}$ composite coating with *in situ* additive introduction was developed, allowing coatings with properties dependent on the additive material and loading. But it is worth noting that the change in properties depends on the additive material, which changes the compared photophysical characteristics, such as flat-band potential (E_{Fb}), charge carrier density (N_D), photocurrent (PCR), and photopotential (OCP), degradation coefficient (k).

Using the developed method and additives of carbon nanoparticles (NPs), it is possible to modify the crystalline phase of the obtained TiO₂ NT, more precisely using hydrothermally treated exfoliated few-layer graphene NPs in

an inorganic electrolyte, and in an organic electrolyte of activated C doped with platinum, the brookite phase ${\rm TiO_2}$ is obtained, which is a unique result compared to the reviewed literature, where brookite phase in anodic ${\rm TiO_2}$ NT coating is not observed.

1.4. Aim and Tasks of this work

This work aims to obtain a photocatalytically active anodic self-organized TiO₂ NT coating for pollution degradation in water and air.

- Investigate the anodization method for obtaining a nanostructured TiO₂ coating in an inorganic electrolyte
- Determine optimal synthesis parameters of anodic TiO₂ coating to improve photocatalytic properties.
- Determine optimal post-treatment parameters of anodic TiO₂ coating to improve photocatalytic properties.
- Characterizing the structural and photocatalytic properties of the obtained anodic coatings.

1.5. Defendable theses

- The developed modification of anodization method by introducing a low voltage step, lower than field assisted TiO₂ nanostructuring voltage, increases the thickness of the dense oxide layer and promotes anatase phase content that leads to an improved photocatalytic properties of synthesized material.
- Developed a novel method for in situ incorporation of nanoparticles into anodic nanotube coatings by combining anodization and electrophoresis, enabling control over photocatalytic activity and crystalline structure while preserving the nanotubular morphology of anodic titania.
- Incorporating hydrothermally treated exfoliated graphene nanoparticles and platinum-doped carbon nanoparticles into anodic titania, as additives in inorganic and organic base electrolytes respectively, enhances the development of brookite phase, improving photocatalytic activity compared to the anatase phase.

1.6. Scientific results and validation

Research and investigation of materials, methods, and properties have been disseminated through various channels. Findings and studies on synthesis methods and materials, used in this thesis, have been published, other investigations of synthesis methods or materials have been published but data not directly used in this thesis. The following list represents work conducted in connection with materials and methods investigated and utilized for this thesis, contributing to its knowledge base.

1.6.1. Reviewed Publications

- 1. <u>Knoks A.,</u> Grinberga L., Kleperis J. "Novel Anodic TiO₂ Synthesis Method with Embedded Graphene Quantum Dots for Improved Photocatalytic Activity" *Coatings*, 14(11), 1407, (2024), 10.3390/COATINGS14111407
- Lesnicenoks, P., <u>Knoks, A.</u>, Piskunov S., Jekabsons L., Kleperis J. "N-Graphene Sheet Stacks/Cu Electrocatalyst for CO₂ Reduction to Ethylene", *Electrochem*, Volume 3, Issue 2, pp. 229–238, (2022), 10.3390/ electrochem3020015
- 3. <u>A. Knoks</u>, J. Kleperis, G. Bajars, L. Grinberga and O. Bogdanova "WO₃ as Additive for efficient photocatalyst binary system TiO₂/WO₃" *Latvian Journal of Physics and Technical Sciences*, 58(6), pp. 24–34, 2021, 10.2478/lpts-2021-0043
- Olins R., Lesnicenoks P., Kleperis J., <u>Knoks A.</u>, Lukosevics I. "Electrochemical exfoliation streamline method for synthesis of nitrogen doped graphene" *Chemija*, 32(1), pp. 9–16, (2021), 10.6001/CHEMIJA.V32I1.4396
- Knoks A., Sika R., Olins R., Lesnicenoks P. "Investigation of carbon nanomaterial influence on photocatalytic properties of TiO₂" Proceedings of the International Scientific Conference Engineering for Rural Developments, 20, pp. 1804–1813, (2021), 10.22616/ERDev.2021.20.TF397
- A. Knoks, P. Lesnicenoks, J. Kleperis, L. Grinberga, J. Hodakovska, J. Klavins, G. Cikvaidze and I. Lukosevics. "Electro-catalytic and photo-catalytic reformation of CO₂ reactions and efficiencies processes (Review)." IOP Conference Series: Materials Science and Engineering, 503(1), (2018), 10.1088/1757-899X/503/1/012009
- 7. <u>A. Knoks</u>, J. Kleperis, L. Grinberga "Raman spectral identification of phase distribution in anodic titanium dioxide coating". *Special issue Proceedings of the Estonian Academy of Sciences*, 66(4), pp. 422–429, (2017) ISSN 1736-7530 (electronic) ISSN 1736-6046 (print), 10.3176/proc.2017.4.19.

1.6.2. Reviewed abstracts

8. <u>A. Knoks</u>, J. Kleperis, L. Grinberga, "Peculiarities of TiO₂ nanotube optical properties" *Riga Technical University 57 International Scientific Conference* "Materials Science and Applied Chemistry 2016 October"; Book of abstracts.

1.6.3. Other related publications

A. Knoks, L. Grīnberga, J. Kleperis, I. Liepiņa, G. Bajārs, Nanostructured TiO₂-based materials with photocatalytic properties / Nanostrukturēti TiO₂ materiāli un kompozīti ar fotokatalītiskām īpašībām. Chapter 6 in the Book "Nanostructured Composite Materials for Energy Storage and Conversion", University of Latvia, Riga, (2019), pp. 124–138, ISBN 978-9934-18-411-6

- Enerģija un Pasaule "Saules gaismas enerģija īpašu materiālu klātbūtnē mazina antropogēno gaisa piesārņojumu" Aprīlis-Maijs (2018) Nr. 2/109, ISSN 1407-5911
- 11. Lisovski, O., Piskunov, S., Bocharov, D., (...), <u>Knoks A.</u> "CO₂ and CH₂ Adsorption on Copper-Decorated Graphene: Predictions from First Principle Calculations" *Crystals*, *12*(2), 194; (2022) https://doi.org/10.3390/cryst12020194.
- 12. Su Y., Xue H., Fu Y., Chen S., Li Z., Li L., <u>Knoks A.</u>, Bogdanova O., Lesničenoks P., Palmbahs R., Laurila M.M., Mäntysalo M., Hammar M., Hallén A., Nordell N., Li J. Monolithic Fabrication of Metal-Free On-Paper Self-Charging Power Systems. *Advanced Functional Materials*, 34(24), 2313506, (2024) 10.1002/adfm.202313506.
- 13. Palmbahs R., Lesnicenoks P., <u>Knoks A.</u>, Vitola V., Kleperis J. Synthesis Method Comparison of N-Doped Carbons for Electrochemical Energy Storage. *ChemEngineering*, 8(4), 80, (2024), https://doi.org/10.3390/chemengineering8040080

1.6.4. Participation in conferences

- A. Knoks, J. Kleperis, L. Grinberga. Graphene-based quantum dots as promoters of the photocatalytic activity of anodic nanostructured TiO₂ nanotube layer, E-EMRS 2023 Fall Meeting, Warsaw, Poland, 18.–21.09.2023., I 55_739
- 2. R. Olins, P. Lesnicenoks, J. Kleperis, <u>A. Knoks</u>, I. Lukosevics, Synthesis of N-doped graphene and it's applications in electronics, 37. Annual ISSP Conference, Riga, Latvia, 23.–25.02.2021, P24
- J. Kleperis, Ingars Lukosevics, Sergejs Piskunovs, P. Lesnicenoks, <u>Ainārs Knoks</u>, Laimonis Jēkabsons, Electrochemical deposition of copper catalyst for CO₂ reduction to ethylene, 36. Annual ISSP Conference, Riga, Latvia, 11.–13.02.2020, P38
- A. Knoks, J. Kleperis, P. Lesnicenoks, G. Kucinskis, L. Grinberga, Annealing atmosphere influence on photophysical properties of TiO₂/GQD system, 36. Annual ISSP Conference, Riga, Latvia, 11.–13.02.2020, P78
- A. Knoks, G. Chikvaidze, S. Piskunov, G. Vaivars, J. Kleperis, P. Lesnicenoks, I. Lukosevics, ATF-FTIR use as theoretical reaction mechanism verification method in determination of CO₂ electrochemical reformation products, 36. Annual ISSP Conference, Riga, Latvia, 11.–13.02.2020, P79
- 6. R. Olins, P. Lesnicenoks, J. Kleperis, <u>A. Knoks</u>, I. Lukosevics, Electrochemical exfoliation streamline method for synthesis of nitrogen doped graphene, Online FM&NT2020, Vilnius, Lithuania, 23.–16.11.2020,P1 14
- A. Knoks, P. Lesnicenoks, I. Lukosevics, Investigation of Anodic TiO₂ in situ
 doping with graphene nanoparticles on photocatalytic activity, 35. Annual
 ISSP Conference, Riga, Latvia, 20.–22.02.2019, P. 67

- 8. P. Lesnicenoks, <u>A. Knoks</u>, I. Lukosevics, K. Kaprans, L. Grinberga, L. Jekabsons, J. Kleperis, Nitrogen Doped Graphene: Conductivity and Gas sensor Properties, 35. Annual ISSP Conference, Riga, Latvia, 20.–22.02.2019, P. 59
- 9. A. Knoks, J. Kleperis, L. Grinberga, P. Lesnicenoks, I. Lukosevics, Influence of TiO₂ in situ doping with graphene nanoparticles on electrochemical properties, Advanced Materials and Nanotechnologies, Palanga, Lithuania, 19–23.08.2019, P. 114
- A. Knoks, J. Kleperis, L. Grinberga, P. Lesnicenoks, Julija Hodakovska, M. Vanags, Electrocatalytic CO2 Reduction into Useful Fuel: Investigation of Electrode Material, 34. Annual ISSP Conference, Riga, Latvia, 20.–22.02.2018, P. 37
- 11. <u>A. Knoks</u>, J. Kleperis, L. Grinberga, Heat Treatment influence on Photocatalytic properties of Anodic Titania, 34. Annual ISSP Conference, Riga, Latvia, 20.–22.02.2018, P. 73
- 12. A. Knoks, J. Kleperis, P. Lesnicenoks, I. Lukosevics, J. Hodakovska, L. Grinberga, G. Cikvaidze, J. Klavins, Photo-catalytic and Electro-catalytic CO₂ Reformation–Reactions and Efficiencies in Separate and Combined Processes (Review), 12th international Scientific Conference on Functional Materials and Nanotechnologies, 2.–5.10.2018, Riga, Latvia, PO-22
- 13. P. Lesnicenoks, I. Lukosevics, L. Grinberga, A. Volkovs, V. Nemcevs, M. Vanags, <u>A. Knoks</u>, A. Dorondo, A. Berzina, J. Kleperis, Frequency modulations in electrochemical exfoliation of FLG material from recycled graphite, 12th international Scientific Conference on Functional Materials and Nanotechnologies 2018, 2.–5.10.2018, Riga, Latvia, PO-90
- A. Knoks, J. Kleperis, L. Grinberga, P. Lesnicenoks, J. Hodakovska, G. Cikvaidze, M. Vanags, A. Volkovs, Spectroscopic investigation of Metal catalyst influence on ElectroCatalytic CO₂ reduction streamline investigation, E-EMRS 2018 Spring Meeting, Strasbourg, France, 18.–22.06.2018, T P2.8
- 15. A. Gudins, L. Daugavietis, M. Zubkins, <u>A. Knoks</u>, M. Vanags, R. Ignatans, J. Kleperis, Growth and Photoconductivity Measurements of The ZnO/TiO₂ heterostructure, 33. Annual ISSP Conference, Riga, Latvia, 22.–24.02.2017, P. 42
- A. Knoks, Ieva Grauduma, L. Grinberga, J. Kleperis, Reduction of Carbon Dioxide and role of Titanium Dioxide in it, 33. Annual ISSP Conference, Riga, Latvia, 22.–24.02.2017, P. 45
- 17. A. Knoks, J. Kleperis, L. Grinberga, Raman Spectral identification of Phase Distribution in Anodic Titanium Dioxide Coating, Functional Materials and Nanotechnologies FM&NT2015, Tartu, Estonia, 24.–17.04.2017. P. 26
- 18. <u>A. Knoks</u>, J. Kleperis, M. Vanags, L. Grinberga, Transition Metal Oxide Heterostructures with Photo-Catalytic Activity, COST-to-BE Fall Meeting 2017, Riga, Latvia 11.–13.09.2017, WG2-6, P. 80
- Ieva Grauduma, <u>A. Knoks</u>, J. Kleperis, Nanostructures Titania for Reduction of Carbon Dioxide, 32. Annual ISSP Conference, Riga, Latvia, 17.–19.02.2016. P. 62

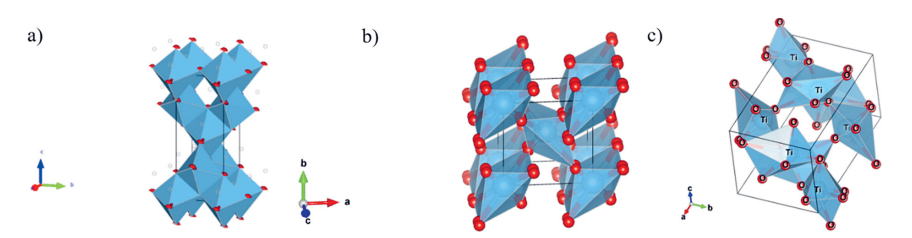
- 20. E. Laivina, K. Gauja, J. Kleperis, M. Zubkins, <u>A. Knoks</u>, Physical and Photoelectric properties of Magnetron Sputtered Titanium Dioxide, 32. Annual ISSP Conference, Riga, Latvia, 17.–19.02.2016. P. 63
- 21. <u>A. Knoks</u>, L. Grinberga, J. Kleperis, Allotropic Modification, Crystallinity and Photoactivity of Titanium Dioxide, 32. Annual ISSP Conference, Riga, Latvia, 17.–19.02.2016. P. 87
- 22. <u>A. Knoks</u>, J. Kleperis, L. Grinberga, Influence of TiO₂ Nanotube Array Synthesis Parameters on Photo-Activity, Advanced Materials and Nanotechnologies 2015, Palanga, Lithuania, 27.–31.08.2016, P. 112
- 23. <u>A. Knoks</u>, J. Kleperis, L. Grinberga, Peculiarities of TiO₂ nanotube optical properties, Riga Technical University 57th International conference MSAC 2016, 21.10.2016, Riga, Latvia, P
- 24. <u>A. Knoks</u>, A. Solovjovs, A. Volkovs, M. Vanags, V. Nemcevs, and J. Kleperis, Research of Direct Methods to Reduce Air Pollution in Street Canyons the Case of Kr.Valdemara Street in Riga, Tartu, Estonia, 9.–12.10.2016, P.
- 25. <u>A. Knoks</u>, J. Kleperis, L. Grinberga, Features of Anodized TiO2 Nanotube growth process, 31. Annual ISSP Conference, Riga, Latvia, 24.–26.02.2015. P. 30
- Rihards Vaivods, Kārlis Lācis, <u>A. Knoks</u>, J. Kleperis, L. Grinberga, Synthesis of TiO₂ Nanostructures for Water Purification, 31. Annual ISSP Conference, Riga, Latvia, 24.–26.02.2015. P. 73
- 27. A. Knoks, L. Grinberga, J. Kleperis, Structural, optical and photo-electrochemical research of anodised TiO₂ nanotube arrays, Functional Materials and Nanotechnologies FM&NT2015, Vilnius, Lithuania, 5.–8.10.2015. P.135
- 28. <u>A. Knoks</u>, J. Kleperis, L. Grinberga, Anodization pre-treatment influence on grows facilities of TiO₂ nanotube arrays, EuroNanoForum 2015, Riga, Latvia, 10.–12.06.2015.
- A. Knoks, J. Kleperis, L. Grinberga, Photoactivity of Anodized TiO₂ Nanostructures, Advanced Materials and Nanotechnologies 2015, Palanga, Lithuania, 27.–31.08.2015, P. 28
- 30. <u>A. Knoks</u>, L. Kuhta, M. Milberga, L. Grīnberga, J. Kleperis, The features of self-assembling TiO₂ nanostructures growth methodology and results, 30. Annual ISSP Conference, Riga, Latvia, 19.–21.02.2014, P. 74
- 31. <u>A. Knoks</u>, J. Kleperis, L. Grīnberga Photophysical Properties of Metal Oxide multilayer films, 30. Annual ISSP Conference, Riga, Latvia, 19.–21.02.2014. P. 19
- 32. A. Knoks, J. Kleperis and L. Grinberga, Synthesis and photocatalytic activity of TiO_2 nanotubes, Functional Materials and Nanotechnologies RCBJSF and FM&NT2014, Riga, Latvia, 29.09.–02.10.2014. P.
- 33. <u>A. Knoks</u>, J. Kleperis, Growth of TiO₂ Nanotubes by Electrochemical Anodization, Advanced Materials and Nanotechnologies 2014, Palanga, Lithuania, 27.–31.08.2014, P. 24

1.7. Literature overview and background

Titanium dioxide (TiO₂) is a widely used material; it has three most common polymorphic phases: anatase, rutile, and brookite, the unit cells of which are respectively shown in Fig. 2 a), b), and c). It is important to note that anodically obtained TiO₂ nanotube (NT) coating has been reported in the available literature in the anatase and rutile phases. Moreover, NT is not found in the brookite phase. The rutile phase is known to be more thermodynamically stable, with a smaller unit cell volume but lower electron conductivity and, thus, photoactivity. As brookite is rarely synthesized, there are no clear comparisons between NT coatings in different phases.

 ${
m TiO_2}$ can be obtained by various methods, including electrochemical anodization, in which a nanostructured self-oriented ${
m TiO_2}$ coating is grown from metallic titanium foil. These coatings have photocatalytic activity. Therefore, they can decompose pollutants, ideally by irradiation with light.

The synthesis of TiO₂ can be carried out by different methods: sol-gel [12], magnetron sputtering [13; 14], pyrolysis [15], laser ablation [16], hydrothermal synthesis [17] etc.; these methods provide thin films or nanoparticles (NPs). It is known that, depending on the structure and size, nanoparticles can be toxic, which is not clearly addressed in the case of TiO2, as there are reports of toxicity [18], where the anatase form is noted to have a more significant effect, but the actual particle size is not mentioned. On the other hand, a large amount of particles suggests toxicity and even the formation of lung cancer in rats [19], but such particles can also be used to eliminate cancer and other cells. So, depending on the size and amount of NPs, TiO₂ can be considered not safe [20], while the advantage of NPs is a large total surface area, relative safety is also of concern. On the other hand, thin films and coatings are safer as there is a lower probability of leaching into the environment, but to compete with NPs, the surface area has to be increased in combination with the option to be reused. It provides lower concern about the material entering the environment. One of the methods for obtaining thin films with large surface area is electrochemical anodization, where it is possible to obtain self-oriented TiO2 NTs [21], which



 $\it Fig.~2.~TiO_2$ unit cell models: a) anatase; b) rutile; c) brookite. All cells were built using VESTA software

allows for an increased surface area compared to a flat coating, increasing photogenerated carrier separation and conduction [22]. Additionally, depending on the electrolyte used, different structural and geometric/morphological properties such as diameter, length, and adhesion are adjustable [22; 23; 24; 25]. A classical model proposes a growth mechanism that is visible in Fig. 3, where the natural dense TiO₂ layer is chemically etched by fluoride ions, forming pits Fig. 3 I b). Applying an electric field promotes the dissolution of this oxide further and deepening of pits Fig. 3 I subfigure c) and d), culminating in the structure of self-organized tubes formed from the wells. As the length of the tubes increases, ion diffusion and oxide growth occur; the anodization process is a state of equilibrium between oxide dissolution and oxide NT formation. Ion migration and oxide growth model on the oxide-metal interface are shown in Fig. 3 II.

Fig. 3 schematic growth mechanism of nanotube coating I stages of development of the most widely accepted model from a) splitting of the dense oxide layer to e) creation of the tube shape, II ion migration within the oxide-metal interface, adapted from [26].

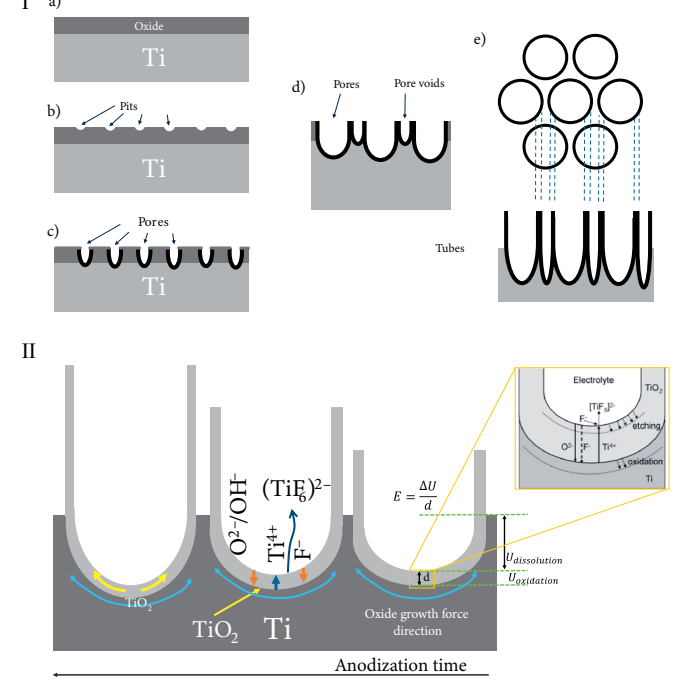


Fig. 3. Schematic growth mechanism of nanotube coating I stages of development of the most widely accepted model from a) splitting of the dense oxide layer to e) creation of the tube shape; II ion migration within the oxide-metal interface, adapted from [26]

Self-assembly of TiO_2 NT layer formation opens up the possibility of obtaining a stable photoactive material with variable properties depending on the geometry [27; 28; 29], coating thickness [29; 30] and the amount of additives [31; 32]. The length and diameter of the tubes affect the photophysical properties, i.e., photocurrent (PCR) and photopotential (OCP), which depends on the position of the conduction and valence band edges and thus the flat band potential ($E_{\rm Fb}$) [33]. At the same time, these properties also depend on the crystalline structure and the composition of phases [34]. Considering that TiO_2 is amorphous after anodization [35] as well as empirical experience, it must be crystallized, achieved by heating the sample in a selected atmosphere and temperature. It should be noted that the temperature ranges and times available in the literature are very different, thus, it is not clear what are the optimal conditions for anodic NTs.

Looking at the semiconductor (SC)-electrolyte interface, we can observe the transfer of charge carriers through this interface, and both the depletion zone on the semiconductor side and the double layer on the electrolyte side are formed. This results in the curvature of the edges of the conduction (CB) and valence bands (VB), as is shown in Fig. 4 a) 2-electrode scheme and b) SC-electrolyte interface. The curvature of the edges of the bands with and without electrolyte containing contamination that should be separated is marked as a red-ox pair. For the purposes of this work, we'll be looking into breakdown of pollutants such as methylene blue (MB), thus, the red-ox pair could be MB, or analogously, it could be water molecule for H₂ production. As can be seen in Fig. 4 a) the decomposable molecule will adsorb on the SC surface with its red-ox potential. In the dark, the Fermi level of the SC equilibrates with the Fermi level of the electrolyte/environment as charges move between the SC and the electrolyte, leading to the bending of the band edges. If the SC is irradiated with electromagnetic radiation whose energy is greater than the SC band gap (E_{gap}), the electron-hole pairs reduce the curvature of the band edges, resulting in a reduced quasi-Fermi level. When this system is illuminated, the photovoltage ΔV_{fot} is obtained, which determines the strength of the electric field, which helps to separate the generated charge carriers for the breakdown of the environmental contamination, where holes provide reduction. At the same time, electrons are driven to the counter electrode through the bulk of the material, here charge carrier separation is crucial for higher efficiency. A detailed pattern of edge curvature is shown in Fig. 4 b), where the effect of the environment and the adsorption of red-ox molecules are plotted with the work function and obtainable potentials. Therefore, the E_{Fb} gives an insight into the additional energy required for the photocatalytic reactions to take place, i.e., the potential at which the injected charges into SC are returned to the environment and the edges of the zones align. Thus, the estimation of E_{Fb} can give insight into material activity.

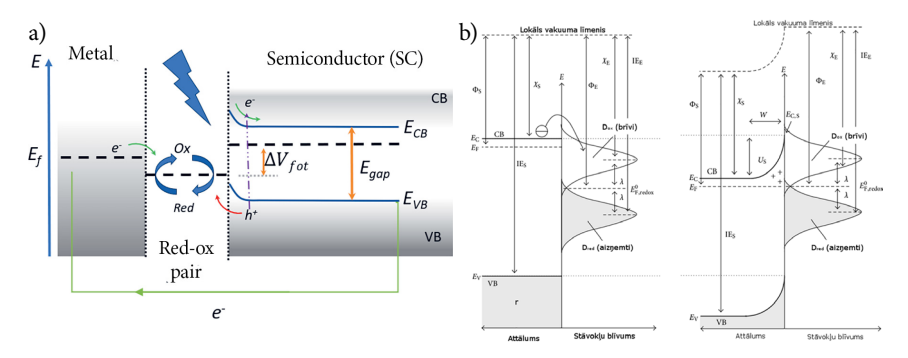


Fig. 4. Schematic representation of band Gap. a) Electrolyte and light irradiation influence on the semiconductor-metal interface, Fermi level shift and charge transfer; b) electrolyte red-ox pair interaction, schematic depiction of charge transfer and resulting band bending, adapted from [36]

Furthermore, in order to improve the photocatalytic properties, several material parameters must be changed; the position of the absorption edge, i.e., $E_{\rm gap}$ make changes in the position of the edges of the zones and achieve greater absorption in the longer wavelength range. In the case of ${\rm TiO_2}$, this would be the visible range since pure ${\rm TiO_2}$ – anatase 3.2 eV, rutile 3.0 eV, and brookite from 3.0 to 3.6 eV, which indicates that the expected effective absorption occurs in the near UV range. So there are several parameters that determine the activity; one should also look at the position of the CB and VB zone edges with respect to the red-ox potential of pollutant, the mobility of the charge carriers, and, as noted by Luttrell et al. the separation of charge carriers in the volume plays a major role in the overall activity, which is manifested, for example, in the higher photoactivity of the anatase phase [37]. Despite the fact that fundamentally we cannot change the $E_{\rm gap}$, functionally, we can form heterojunctions and material combinations that effectively shift the absorption edge due to increased absorption or due to the introduction of new states in the bandgap.

For example, in the existing model, the deposition of WO $_3$ on TiO $_2$ should increase carrier separation and increase the number of generated carriers, as measured by PCR and photocatalytic activity. For example, Hoffman et al. proposed model states that a layer of electrons exists in SC NPs [38]. With sufficient mixing, the particles collide, shrinking this layer, resulting in composite-semiconductor charge transfer. The charge transfer mechanism in a WO $_3$ / TiO $_2$ composite occurs when the hexavalent tungsten captures an electron from the TiO $_2$ photo-charge excitation process [39; 40] and switching to pentavalent tungsten. The oxygen in the system then converts the tungsten from pentavalent back to hexavalent tungsten.

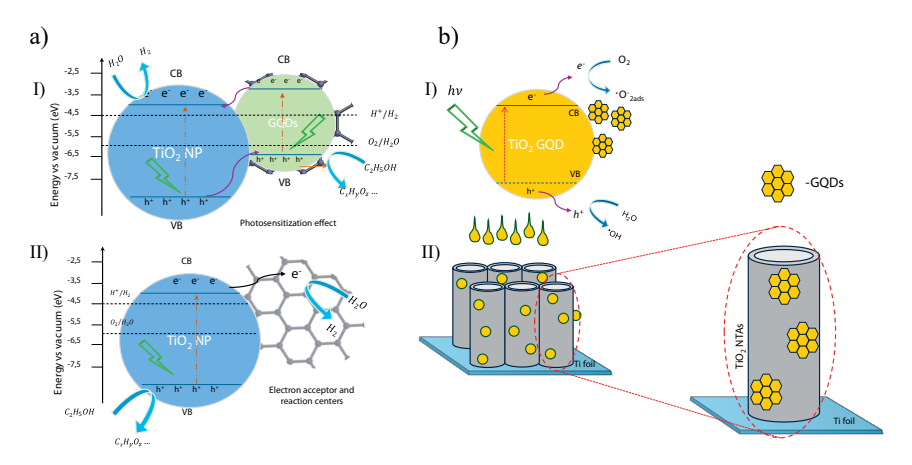


Fig. 5. Schematic representation of TiO₂ with CNP materials. a) I) GQD acts as hole concentration center and increases absorbance; II) graphene works as electron concentration center for increased charge separation, images adapted from [41; 42]. b) schematic GQD influence on TiO₂ including induced e⁻-h⁺ pair transition; II) Schematic depiction of NT impregnation with GQD, image adapted from [43]

Alternative methods to increase activity are also found; the introduction and addition of various quantum dots (QDs) are gaining popularity; it is worth remembering that some QDs are highly toxic, so one should look at the choice of sustainable and safe abundant materials, such as carbon NPs. In Fig. 5 we see a proposed mechanism for the influence and interaction of QDs with the environment. This case examines TiO₂ NPs with graphene quantum dots (GQD) [41; 42], on the other hand Fig. 5 b) reviews the anodic coating of NT impregnated GQD. Incorporating these particles into an anodic nanostructured TiO₂ coating by impregnation was investigated by Gupta et al., who found an overall increase in the set of photoelectrochemical properties, including MB decomposition. It is worth noting that no change in the crystalline structure of TiO₂ NT was detected after the addition of GQDs [43].

2. EXPERIMENTAL METHODS AND DESCRIPTION

2.1. Determination of photoelectrochemical properties

A 3-electrode cell was used for the determination and measurements of photoelectrochemical properties and parameters, and overview is depicted in Fig. 6, overall setup a) where the working electrode is the TiO_2 NT sample, the supporting electrode is blackened platinum foil, and a calomel (Cl^-4M)| $Hg_2Cl_2(s)$ |Hg(l)|Pt) electrode (SCE) is used as a reference electrode.

Photocurrent (PCR), photopotential (OCP), and Mott-Schottky (MS) analyses were conducted using a Radiolab Analytica VoltaLab PGZ 301 potentiostat for inorganic samples and a Metrohm Autolab PGSTAT302N for samples synthesized in an organic base electrolyte. The experimental setup, illustrated in Fig. 6 b) and in Fig. 6 e), includes a potentiostat, a computer for data acquisition and processing, and a cell equipped with light modulation (chopping) capability. Measurements were performed using NaOH or KOH electrolytes, purged with nitrogen or argon for 15-20 minutes under standard conditions. The light source spectrum is shown in Fig. 6 c), and the measured OCP, PCR, and MS data are presented in Fig. 6 d). Light modulation was used for OCP and PCR measurements with a set period of dark and light cycles of 5 and 60 seconds to determine the activity of samples. During these measurements, illumination was provided by a high-pressure xenon lamp, 10 mW/cm², spectrum shown in Fig. 6 c). The lamp's manufacturer power rating is 150 W, with cut off UV spectral part, that is a B type lamp. Therefore, this work uses data on the obtained TiO₂ NT activity in the visible range at all times.

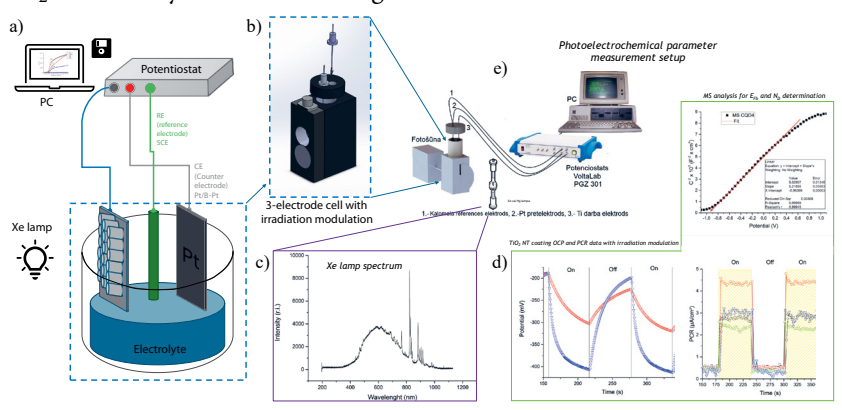


Fig. 6. Experimental device schematic for electrochemical measurements a) 3 electrode schematics for OCP, PCR, MS measurements; b) photocell with irradiation modulation capabilities; c) Irradiation lamp spectrum; d) measurement outcome data OCP, PCR, MS; e) the computer representation for data acquisition and processing

Light modulation enables the estimation of generated charge carriers, recombination rates, and charge kinetics. Prior to each measurement, the electrolyte was purged with inert gas (N_2 or Ar) to minimize dissolved oxygen, reducing photocharge quenching by the electrolyte and providing a more accurate characterization of the material's OCP and PCR values. To find the $E_{\rm Fb}$, Mott-Schottky analysis is performed. By performing the MS analysis, it is possible to obtain not only the $E_{\rm Fb}$, using Eq. (1), in addition to determine the depletion zone and charge carrier density, as described in [44].

$$\frac{1}{C_{Sc}^2} = \frac{2}{\epsilon \epsilon_0 e N_D} \left(E_{ex} - E_{Fb} - \frac{k_B T}{q} \right)$$
 (1)

where C_{SC} – is the resulting coating capacitance, ϵ – TiO_2 dielectric constant, ϵ_0 – permittivity of free space, e – electron charge, N_D – charge carrier density, E_{ex} – bias potential, E_{Fb} – flat band potential, k_B – Boltzmann constant, T – temperature in Kelvin. Knowing these values, it is also possible to determine the concentration of charge carriers N_D , which can be expressed as Eq. (2)

$$N_{\rm D} = \frac{2}{\varepsilon \varepsilon_0 e S^2 k_{\rm sl}}$$
 (2)

where ϵ – dielectric constant of TiO $_2$, ϵ_0 – permittivity of free space, e^- – electron charge, k_{sl} – determined slope coefficient of the linear part found from MS analysis, S – geometric surface area of the coating. E_{Fb} and N_D are parameters, similar to OCP and PCR, with which we can compare the photophysical properties of the samples and evaluate the potential for catalytic activity, as well as qualitatively compare the samples.

2.2. Study of structural and optical properties

The crystalline structure is a crucial aspect of sample characterization and is carefully considered in relation to synthesis parameters. This thesis examines the influence of synthesis parameters on photophysical properties, highlighting the significant role of crystalline structure and phase composition, particularly the specific TiO₂ phase or phase mixtures. Raman spectroscopy and X-ray diffraction are used to analyze the crystalline structure. Since anatase is regarded as the most photocatalytically active phase, achieving a higher proportion of anatase is a primary objective for enhancing photocatalytic activity. The classical TiO₂ anatase Raman spectrum has six Raman-active fundamental vibrational modes: three E_g , with peaks resp. $E_{g(1)} - 144 \text{ cm}^{-1}$, $E_{g(2)} - 197 \text{ cm}^{-1}$ un $E_{g(3)} - 639 \text{ cm}^{-1}$, two B_{ag} modes at $B_{1g(1)}$ – 399 cm^{-1} un $B_{1g(2d)}$ – 519 cm^{-1} , in addition to A_{1g} – 513 cm^{-1} [45; 46; 47]. The covalency/length/frequency interrelation shows that the Raman modes at 640 cm⁻¹, 517 cm⁻¹, and 397 cm⁻¹ correspond to mildly distorted TiO₆⁸⁻ octahedron, in the case of anatase with calculated bond sizes: Ti-O 2x 1.89 Å, 3x 2.02 Å and 2.14 Å. On the other hand, O-O covalent interaction in literature is assigned to 246-351 cm⁻¹. Sharp modes at 197 cm⁻¹ and 144 cm⁻¹ ascribed to Ti-Ti bonds with lengths around 2.96 Å (respectively calculated 2.89 and 2.96 Å) [48].

Given the depth limitations of Raman scattering, the crystalline structures within the sample volume were determined using X-ray diffraction (XRD). The XRD data were analyzed by fitting to known crystalline phases or phase mixtures, using libraries such as ICDD and comparing the results with published literature data [27; 49; 50; 51; 52; 53; 54], typical anatase phase Bragg peaks are at $2\theta = 25.4^{\circ}$, 37.9° , 48.2° , 54.0° , 55.2° and 62.73° respectively corresponding to (101), (004), (200), (105), (211) and (204) [55]. For rutile and brookite analogs, direction indices have been found and compared with literature data. Further, the designation of phases will be used as A – anatase, R – rutile, T – titanium, and B – brookite. Considering that the NT coatings were obtained on a metallic Ti foil, strong T peaks are visible in the diffractograms of the samples.

Optical absorption edge determination

To assess the optical properties of the samples, a Tauc plot was employed to determine the optical absorption edge of the coating. This was achieved using Kubelka-Munk (KM) transformations based on reflectance spectra (R_{∞}) captured in a diffuse reflectance sphere. The spectra were measured with a UV-VIS-NIR spectrophotometer (Shimadzu SolidSpec-3700). The applied KM transformation is given in Eq. (3):

$$\alpha = \frac{(1 - R_{\infty})^2}{2R_{\infty}} \tag{3}$$

The Tauc plot is used to determine the optical absorption edge, effectively $E_{\rm gap}$, employing KM transformation and the absorption coefficient α . Historically, studies of germanium optical properties determined that the absorption edge of semiconductors can be determined using the optical absorption spectrum. At the same time, it was also determined that it can be found by extrapolating a linear approximation from the absorption spectrum after constructing a Tauc graph, where applying Eq. (4) and plotting the dependence of the absorption coefficient on the photon energy [56; 57; 58].

$$\alpha h \nu = \alpha_0 (h \nu - E_{gap})^{1/n} \tag{4}$$

To obtain the optical absorption edge an approximation $(\alpha \cdot h \cdot \nu)^{1/n} = 0$ is used, it should be noted that TiO_2 is an indirect bandgap material; thus, n is 2.

Methylene blue degradation - determination of photocatalytic activity

The MB degradation coefficient k_i and the amount of degraded MB C_i are used to characterize the photocatalytic properties of a given sample. By comparing k, it is possible to validate the activity of the coating and, thus, the synthesis parameters for the creation of a self-sufficient photocatalyst for the decomposition of environmental pollution. k determination and measurement schematic are visible in Fig. 7, where a) a MB solution (0.034 mM in this work) is placed in the optical cuvette with the TiO_2 sample. As shown in Fig. 7 b) the cuvette is irradiated with Xe light for a certain period, then at set

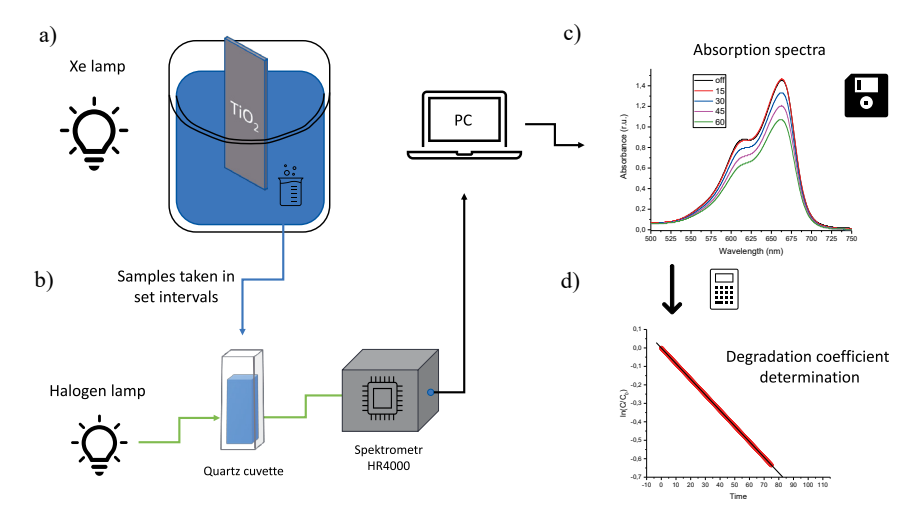


Fig. 7. Schematic representation photocatalytic investigation of TiO_2 samples, MB decomposition experimental setup. a) MB solution with an inserted sample is irradiated for a certain time; b) the absorption spectrum of the solution is measured in set time intervals; c) the change in the intensity of the absorption peak; d) the degradation coefficient is determined as slope of $ln(C_i/C_0)$ vs time plot

time intervals a visible light absorption spectrum of MB solution is measured. Fig. 7 c) shows absorption spectrum change in time, where the peak intensity at 664 nm is determined, the intensity decrease indicates decolorization and MB decomposition. The measurement is repeated with selected time intervals and by comparing the decrease in the concentration over time gathering C_i/C_0 plot. Fig. 7 d) shows the determination of the degradation coefficient k from $\ln(C_i/C_0)$ vs Time plot as the slope coefficient. This procedure validates the determination of the photocatalytic activity of the catalyst, including background determination to exclude its influence.

2.3. Synthesis of materials and samples

2.3.1. Obtaining TiO₂ NTs by electrochemical anodization

Materials available in the laboratory were used without additional purification. Titanium foil with thickness of 0.25 mm (Alfa Aesar, purity 99.9%) was used as the basis for growing TiO₂. 85% H₃PO₄ (Penta), 60% HNO₃ (Enola), ethylene glycol (EG) (Sigma-Aldrich), NH₄F (Sigma-Aldrich), and other chemicals available in the laboratory were used. Sample preparation begins with cutting the base from foil in sample sizes; the average size of the base is 1.5 cm², where the geometric area of anodization is such that final geometric samples size is 1 cm².

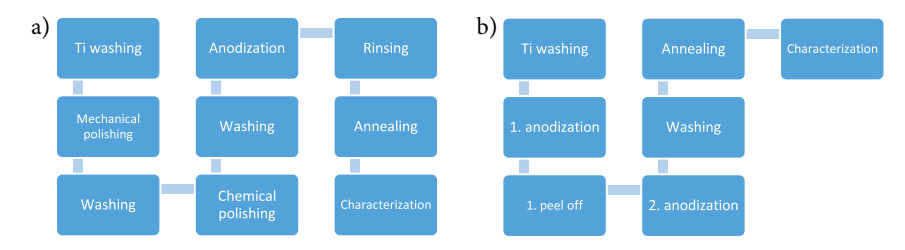
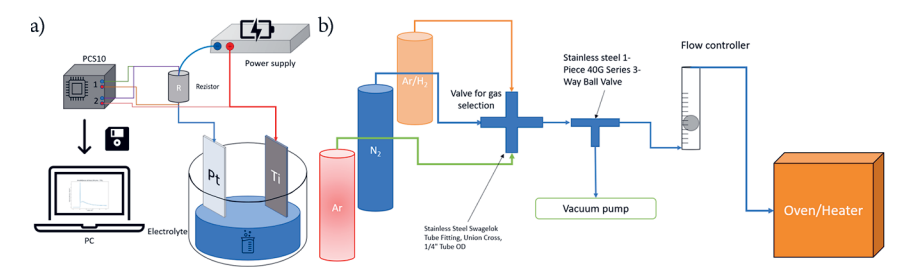


Fig. 8. Sample preparation flowchart a) inorganic electrolyte base and b) organic electrolyte base



 $\it Fig.~9.$ a) Schematic representation of anodization experimental setup; b) Sample annealing/heating experimental setup with option of gas selection

The samples were synthesized using different electrolyte compositions. Inorganic base electrolyte, mainly based on deionized water and acid (H_3PO_4 , H_2SO_4 , HNO_3), where the necessary concentration of fluorine ions is selected at the beginning, the necessary amount is calculated and weighed, then the electrolyte is mixed. The composition of the organic electrolyte mainly contained a solution of EG and NH_4F with a selected concentration of fluoride ions and the amount of water was optimized for best NT outcome. This summary focuses on the main results.

The sample preparation flowchart is visible in Fig. 8 a) inorganic base and b) organic base sample synthesis, whereas sample anodization setup can be seen in Fig. 9 a). All synthesized samples in this work are amorphous; thus, annealing is necessary for crystalline TiO₂. Annealing was carried out in muffle or tubular furnaces at various temperatures and atmospheres, the schematic setup is shown in Fig. 9 b). TiO₂ anodization using the developed in situ additive introduction method with carbon NP additives was performed in an inorganic electrolyte in double anodization, wherein the first step of 25V was supplied for 25 minutes, then the anodization was repeated in the second step by supplying 25V for 90 minutes, in an electrolyte containing additive particles in different concentrations. Additive concentrations varied from 0 to 4 mL of dispersed particles at concentration of 1 mg/mL.

Anodization in an organic electrolyte was carried out using a double anodization with the removal of the first NT layer by the peel-off method, which is discussed below under the results.

2.3.2. Synthesis of Additive Carbon Materials

As for the introduction of additives, there are two ways: to use commercial material or to synthesize the additive materials; in this case, some CNPs were synthesized and compared to commercial material to approve the application of the acquisition method for photocatalytic applications. Let's start with the synthesis parameters described and published in joint work [59]. Exfoliated multilayer graphene particles, hereafter denoted as G, exfoliated nitrogen-doped graphene particles, hereafter denoted as NC, and hydrothermally treated G particles, hereafter denoted as H, were synthesized and added into anodization electrolyte to synthesize composite TiO₂ coatings. As mentioned above, in the chapter on absorption edge identification, introducing these additives into NT could increase light absorption and separation of generated charge carriers, and thus catalytic activity.

The description of the synthesized materials and the acquisition parameters are visible in Fig. 10. Using the electrochemical exfoliation method, graphite electrodes were placed in 800 mL electrolyte, pulsed voltage was applied to electrodes, changing between +10 V and 0 V every 30 seconds. Graphite was exfoliated for 27 h in an electrolyte based on $\rm H_2SO_4$ to obtain G material. Separately graphite was exfoliated in 1 M NaN3 to obtain NC material, followed by sonication of the exfoliated fraction and stepwise filtering and washing. In the case of G, after filtering it was reduced in Ar/ $\rm H_2$ flow at 900 °C for 4 hours. H synthesis was carried out via hydrothermal treatment of G particles as shown in Fig. 10.

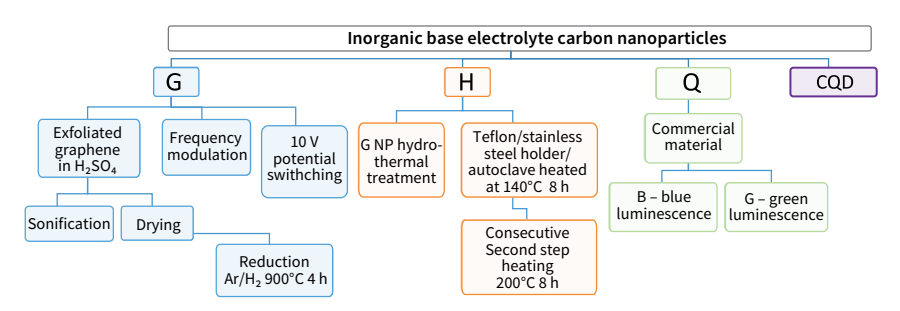


Fig. 10. CNP synthesis flowchart for use as additives for inorganic base electrolyte

3. RESULTS AND DISCUSSION

3.1. TiO₂ NT synthesis in an inorganic electrolyte

The disadvantage of the classic one-step anodization technology in an inorganic electrolyte is the long NT coating growth time, which under normal conditions can be measured in hours [60; 61], assuming Mor et al. proposed growth model we get the classic form of current-time transient, where the electric field, due to applied voltage, increases the oxide layer, followed by the dissolution of the oxide and formation of pores, which further grow into self-oriented tubes [26].

At the beginning of the anodization process, Ti is washed and transferred to an electrolyte in an oxygen-containing environment; thereby, there is the natural titanium oxide layer. Applying a voltage to the Ti base promotes the growth of TiO_2 , and depending on the applied voltage and electrolyte, the NT coating may or may not form. The dense oxide layer will form if the applied voltage is too low for field-assisted anodization. In addition, for nanostructuring to take place, there must be some oxide etching, some ions that would form soluble compounds such as the aforementioned TiF_6^{2-} ; in literature comparisons can be found where only a dense oxide layer is formed without the presence of F^- ions [23]. By applying at least a minimum necessary voltage in the subsequent anodization stages allows for a more even distribution of the electric field, thus facilitating the formation of pores of the same size and the growth of their side edges, which, as a result of self-organization, creates a uniform tubular TiO_2 coating.

In the classical model, the initial state of the natural oxide is assumed to be initiated without considering the parameters of this layer. It is not known what will happen if this process is divided into several stages without exceeding the anodization voltage limit. The first part of this thesis is focused on the modification of the classic anodization by separating the process into two steps. Introducing the first step of low voltage (1–9 V) application, where the growth rate of the dense oxide is higher than the chemical dissolution without field-assisted ion migration through the oxide for active dissolution. The second step is the application of the anodization voltage, e.g., in H₃PO₄, NaF, DIW electrolyte 20 V, 25 V, and 30 V were tested, which promotes active ion migration and consecutive self-organization and growth of nanostructures. A schematic representation of the steps of the two-step method, along with the current-time transient, is shown in Fig. 11.

Thus, the anodization process can be divided into 3 parts. I – low voltage step and oxide growth on the surface Fig. 11 a) and b), II – increasing the voltage up to the anodization voltage, followed by a rapid increase in the current density, and faster growth of the oxide and a subsequent drop in the current density due

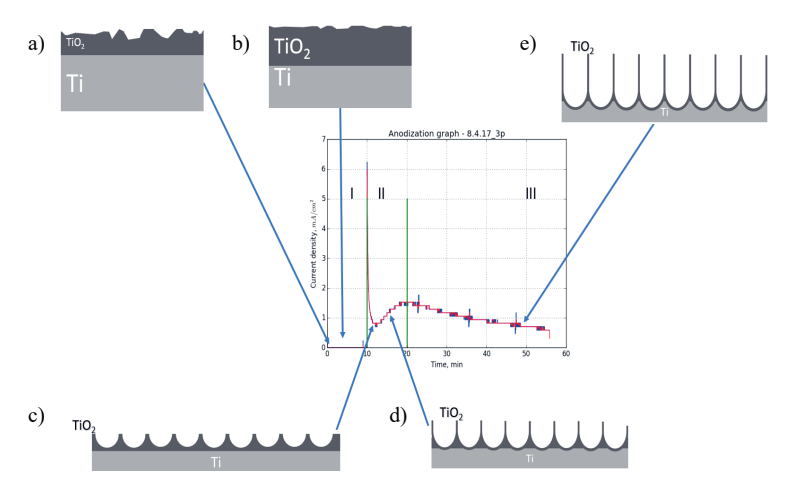


Fig. 11. Current time transient of modified two step anodization. I natural oxide growth, II pore formation, III tube development and growth. a) Natural oxide layer b) first step of anodization – oxide formation promoted by low voltage c) oxide dissolution and formation of holes d) Holes turn into pores e) Pores grow and tubes are formed on their edges

to increased resistance, chemical oxide etching and pore formation Fig. 11 c) and d), followed by a decrease in resistance and, therefore, an increase in current density with subsequent field-promoted oxide growth and dissolution, III – increase in pore depth, the transition from Fig. 11 d) to e) followed by growth of the tubular structure and increase in resistance/decrease in current density. A detailed description of the process, including a description of ion migrations and reactions, can be found in the main thesis work chapter on the description of anodization.

The current-time transient provides an indirect method to monitor the growth process. As shown in Fig. 11, the immediate application of potential causes a sharp increase in current density, followed by a rapid decrease due to oxide formation. The subsequent pore formation reduces resistance, leading to an increase in current density and resulting in variations in surface morphology. In both classic anodization and modified two-step anodization, the nanotube (NT) coating surface is partially covered with a dense TiO₂ layer. Fig. 12 a) and 12 b) illustrate closed tube surfaces, while Fig. 12 c) shows open tubes with partial coverage by a dense oxide layer. In Fig. 12 d), larger islands of dense oxide cover the NT coating, with some areas still partially coated by a dense oxide layer.

One of the important components in evaluating modified anodization is the premise of the more uniform oxide layer. We can estimate the total surface roughness depending on the duration of the low-voltage application and compare it with a classic anodization sample. Fig. 13 shows that the surface morphology

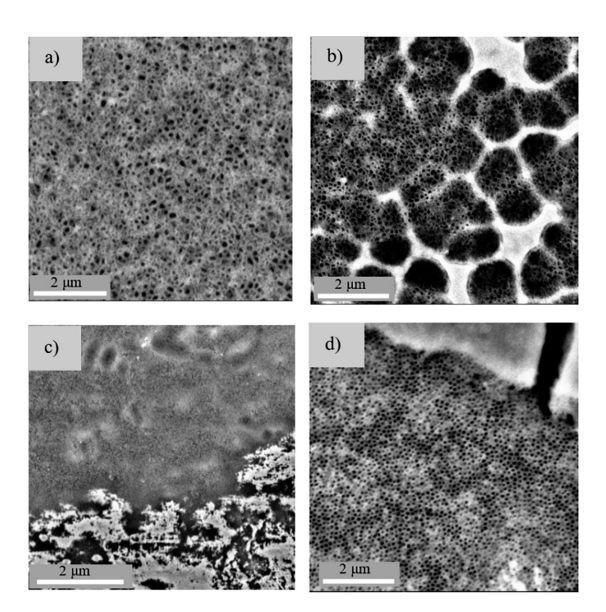


Fig. 12. SEM micrographs of anodic coatings. a) semi regular NT; b) NTs partially covered with dense oxide; c) NTs with islands covering NT openings; d) partially covered NT coating

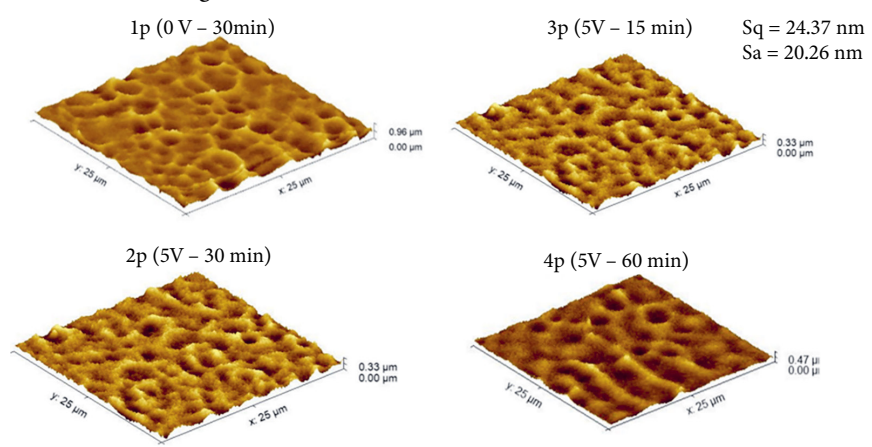


Fig. 13. AFM images of samples with various anodization time. a) classical anodization provides with median roughness around 66.8 nm, b) through d) samples with smoother morphology with median roughness under 50 nm

changes depending on the presence of the low voltage step and its duration. The sample without low voltage (1p) has a more developed average roughness of 66.86 nm compared to 38.19 nm (2p) for the sample with low voltage step.

Therefore, it can be concluded that using the modified anodization with the low voltage step provides significantly smoother sample morphology; using the low voltage develops a more pronounced morphology microstructure in the sample. When held at 5V, the surface has less morphological structure, while anodized without low voltage, the surface morphology is rougher (with larger changes in surface height "valleys and hills"). On the other hand, comparing the effect of anodization time on the surface roughness with the use of the low step, it can be seen that more changes in the surface morphology were obtained at 60 minutes of anodization.

3.1.1. Low voltage effect on crystalline structure

The effect of anodization time on the crystalline structure of obtained samples, can be seen in the diffractogram in Fig. 14 a) and phase ratio in Fig. 14 b) for samples annealed in air at 450 °C. In all cases, some amounts of A and R is gained, but primarily, samples are in the anatase phase. Increasing anodization time increases the proportion of anatase, as can be seen in Fig. 14 b) with an increase in relative intensity of A(101) vs. R(101). As is expected that phase composition is dependent on the relative intensity, with the subtracted background. To a certain extent, this makes sense as the anatase unit cell is larger than rutile, and with higher anodization time, there is a higher available layer thickness.

By increasing the anodization time, we can increase the amount of anatase; on the other hand, the effect of the low voltage step is shown in Fig. 15. In these XRD results, we see the composition of this series, where the samples were obtained using a low voltage step from 0 (thus classically anodized) to 15 minutes with the following anodization voltage of 20V for equal time. All samples exhibit A (101) and R (101) peaks, as can be seen Fig. 15 a). The ratio of their mutual intensities is plotted in Fig. 15 b), where relative intensities are

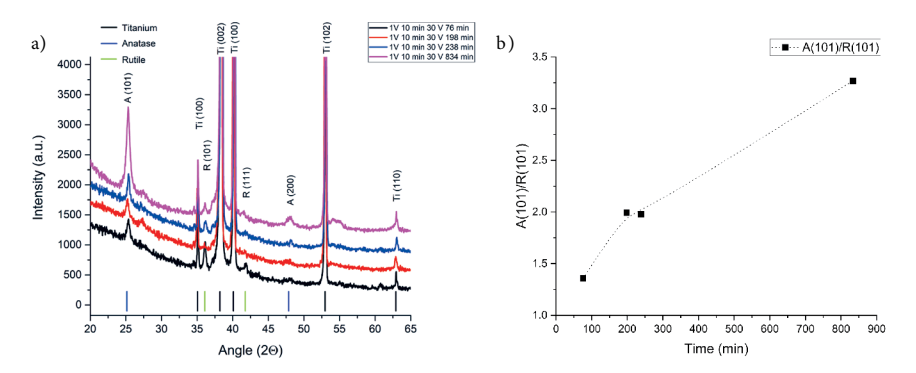


Fig. 14. Anodization time influence on crystalline structure. a) XRD diffractograms of samples with various anodization time; b) Bragg peak of A/R relative intensity comparison depending on anodization time

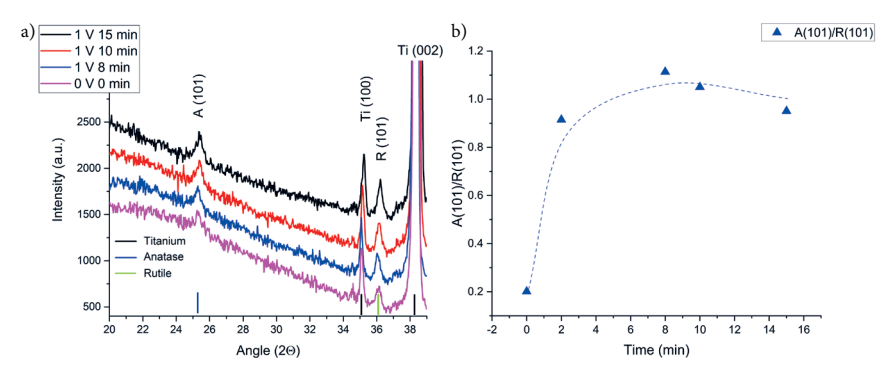


Fig. 15. Comparison of XRD diffractograms and relative A and R intensities: a) XRD of samples with modified two-step anodization with low voltage step of 1 V versus classic one-step anodization with subsequent anodization voltage of 30 V for all samples; b) Plot of the characteristic phase ratio as a function of the low voltage step

compared, and thus the crystalline structure of the obtained coating slightly changes with the introduction of the low voltage step, the ratio of crystalline phases obtained at different times does not change significantly when using the IV low step; on the other hand, it is clear that the amount of A phase is larger than in classical anodization, further substantiating previous result.

One of the parameters that can be easily changed in the electrolyte is the concentration of fluorine ions; in this case, a concentration of F^- significantly affects the formation of the obtained structures and the growth of NT coating. When high concentrations of fluoride ions are used, the resulting tubes begin to disintegrate and break, as can be seen in Fig. 16 a) and b), both from the degradation and partial separation of the upper layers, where deformations of individual tubes and holes in the walls are visible. It is worth noting that the walls/edges of the individual tubes with wavy growths Fig. 16 c) can be explained by the formation of oxide growth and mechanical pressure buildup, as shown in Fig. 3 II; an alternative mechanism was proposed by Regonini et al. [47], proposed a mechanism involving cavitation within the dense oxide layer; however, this theory lacks substantial support from most research in the field.

Considering that such lower quality or torn tubes are obtained, it is necessary further to optimize the quality of the methodology and coatings. It is possible by introducing tube "seeds", but the method should still be simplified, contrary to the classic implementation of NT seeds. Considering the anodization process, it becomes clear that spherical formations should remain on the Ti substrate after anodization, which could be used as finished pores Fig. 3 b)–c) or Fig. 11 in stage II. This means that the anodized NT coating needs to be removed first. The NT layer of the first anodization can be removed; it is known from the literature that this can be achieved with various techniques, such as ultrasound [62], electrostatic polarization, etching, or secondary anodization [63; 64].

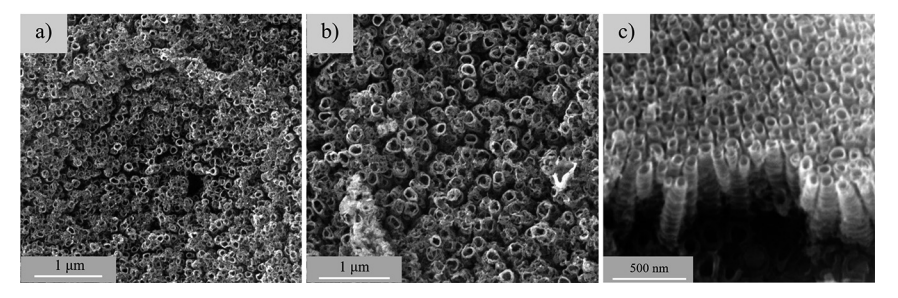


Fig. 16. SEM micrographs of TiO₂ NT with open tube surface and tube side surface. a) and b) shows partial dissolution and breaking of tubes; c) shows a side view of NT coating and visible grooves on the tube walls

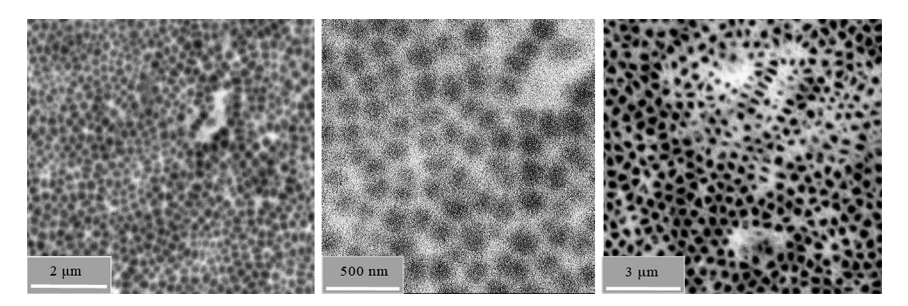


Fig. 17. SEM micrographs of a) and b) Ti surface after anodization, spherical seed are left on the surface; c) double anodization results in a coating with more open tube surface

After removing the first layer, the formed pores remain open, based on which the next NT layer will grow, as mentioned above.

In Fig. 17 a) and b) the morphology of the Ti substrate after NT removal is shown, while Fig. 17 c) shows SEM image of the resulting NT coating, where we see a uniform NT coating with an open tube surface. It is important to note that the adhesion of NT coatings obtained in an inorganic electrolyte is significantly higher compared to the coating obtained in an organic electrolyte, as assessed by the removal efficiency of this NT layer. In the case of an organic electrolyte, a simple methodology is applicable, which will be elaborated further. In contrast, the removal of NT coatings obtained in an inorganic electrolyte is technologically more complex.

 ${\rm TiO_2}$ nanotubes grow so that the axis of the tube coincides primarily with the crystalline (101) direction, where the explanation is the surface energy of the plane [65; 66; 67]. Fig. 18 A) shows high-resolution transmission electron microscope (HRTEM) images with crystallite orientation visible starting from tube overview in a) into various parts of the tube walls b) through d). It shows

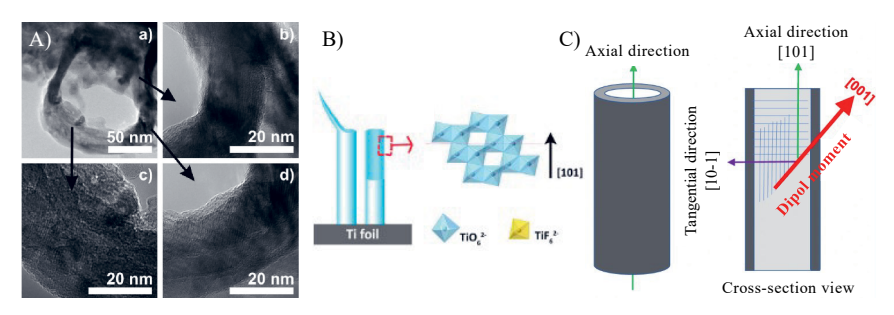


Fig. 18. A) HRTEM images of tube openings from above showing the crystalline structure through the entire tube wall, image taken from Albu et al. [68];
B) Orientation of the crystalline structure of nanostructured NT-coated tubes, position of octahedra; C) cross-sectional diagram of tube and tube with crystalline direction, adapted from [66]

that heated nanotubes can crystallize in a specific orientation. The crystallites can reach sizes on the order of magnitude of tens to hundreds of nanometers as shown by Albu et al. [68]. While Fig. 18 B) shows a schematic representation of the directions, respectively, the orientation of the octahedra or the specifically identified axial [101] direction and Fig. 18 C) shows collinear dipole moment in the [001] direction, which results in its total projection to the [101] direction and thus the total energy of the system as seen in [69]. A similar result is obtained when a thin layer of TiO_2 is applied to an existing tubular system [66; 70].

This explains why we see such a pronounced A(101) peak in the XRD data, and we can also qualitatively assess the thickness of the NT coating and the morphology of the tubes. Rutile is known to consist of a TiO₆ octahedron connected to 10 neighboring octahedra, two with faces and eight with vertices, while anatase TiO₆ octahedra is connected to 8 neighboring octahedra, four with faces and four with vertices, as we saw in Fig. 2 and found in the literature, such as Cui et al. [71] or Seremak et al. [72]. The comparison of the obtained results shows that introducing the first step and extending the anodization duration increases the proportion of the anatase phase in the samples. This is facilitated by the growth of a dense oxide layer, from which a self-oriented NT coating forms during anodization. Furthermore, considering the unit cell formation energy, which is lowest (0.44 J/m²) for the TiO₂ NT crystal plane, and the difference in unit cell sizes between polymorphic phases – where the anatase unit cell is 2.2 times larger than the rutile unit cell – the initial step contributes to both the thickening of the dense oxide layer and the increased proportion of the anatase phase in the NT coating.

In literature, samples heated for shorter times obtained in an electrolyte with the presence of $\rm H_3PO_4$, but with HF concentrations are also found, such as Yoo et al. work, where the resulting coating is amorphous after anodization, but when heated to 450 °C, a mixture of phases appears, which already at 500 °C

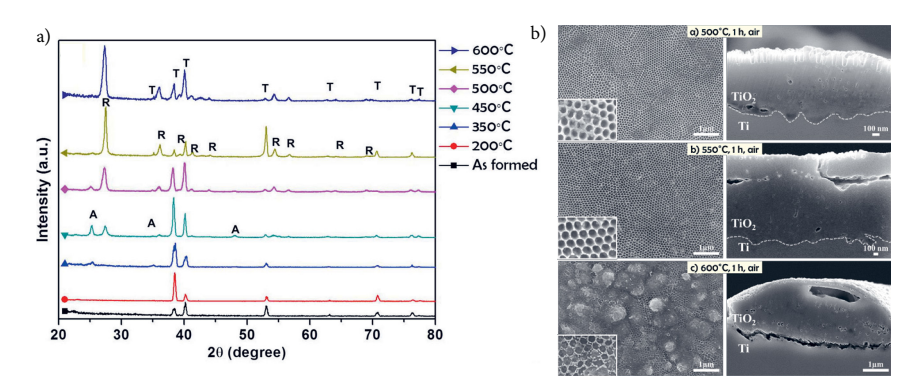


Fig. 19. Yoo et al. examined the composition of anodic TiO₂ phases depending on annealing temperature. Samples obtained in organic electrolyte with HF content heated at different temperatures in air atmosphere; b) SEM micrographs of thermal oxide layer formation under the NT coating [73]

is predominantly in the rutile phase [73], where it is unambiguously stated that ${\rm TiO_2}$ crystallization starts from the formation of a thermal rutile phase layer on the metal/oxide interface, directly under the obtained NT coating, where depending on the heating temperature and duration, this layer grows in thickness and rutile intervenes in the structure of self-organized tubes, breaking them up, as it is visible in Fig. 19 [73]. Too and colleagues also referred to the heating of pure metallic titanium in an air atmosphere, where they showed the formation of anatase from 276 °C. In comparison, the appearance of the rutile layer from 444 °C, thus observed the temperature of anatase/rutile layer mixtures in the range of 450 to 700 °C. It should be noted that the oxidation was performed on pure titanium for 48 hours in a dry-air atmosphere [74].

So we can see that titanium heated in air atmosphere will preferentially form a rutile layer with a distinct R(110) Bragg peak visible in XRD, while A(101) will not be observed even at higher temperatures [75]. On one hand, in the anodic ${\rm TiO_2~NT}$ coating, there will be a phase transition from initially amorphous to the anatase phase, where both the crystallization temperature and further anatase-rutile phase transition point depend on the heating temperature, time, and also the atmosphere.

On the other hand, the XRD analysis of the samples in this study also reveals a dependence on the synthesis parameters, as observed earlier. Notably, most samples synthesized in inorganic electrolytes do not exhibit the R(110) peak in the XRD data, indicating the absence of a thermal rutile layer, except for a slight appearance at longer anodization times. It is important to note that Raman spectroscopy provides insights into the structural composition of the top layer of the coating, as the laser penetration depth is shallow and does not show a significant presence of rutile.

The developed modified two-step anodization method allows variation of sample morphology depending on the first step voltage, duration and subsequent anodization voltage. Low voltage step influences the synthesized anodic titania growth dynamics, allowing smoother morphology compared to classical anodization. Low voltage step introduction allows changes in the crystalline structure of synthesized anodic titania; this anodization modification allows higher content of the anatase phase in the anodic titania due to an increase in dense oxide layer thickness.

3.1.2. Photocatalytic properties

To evaluate the photophysical properties and low voltage step influence on said properties, a comparison of OCP and PCR can be drawn. Even though we see some correlation between PCR and OCP, we should look for a combination of both maximum values. In Fig. 20 a) we see the OCP and PCR values depending on the value of the low voltage step, where 5V step shows the highest parameters; all low voltage steps are shown in Fig. 20 b) we can see that the 5 V step shows the high combination of parameters, although it is worth noting that these results are not specifically divided by heating temperature, atmosphere, and time, though marks/reveals the overall trend.

Optical properties of samples depend on the synthesis parameters, including low voltage introduction. We can evaluate the totality of the optical absorption edge position of all samples, including the two-step anodization parameters. As can be seen in Fig. 21 a), the distribution of values is rather large, but the median value corresponds to the anatase $E_{\rm gap}$ value; there is a dependence on the synthesis and post-processing parameters, too. As we see in Fig. 21 b), even just separation by the heating atmosphere shows sufficient dispersion within this parameter. At the same time, the average values still tend to correspond to

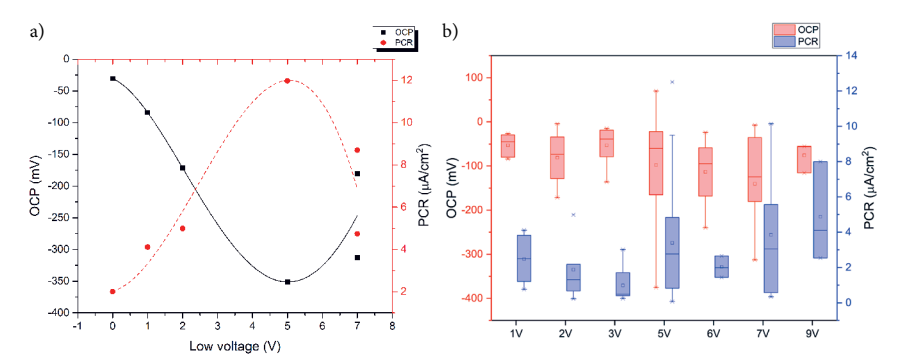


Fig. 20. a) OCP and PCR value dependence on the low voltage step from 2 V to 8 V and anodization voltage of 20 V for 70 min; b) Summary of all synthesized sample OCP and PCR values using modified anodization

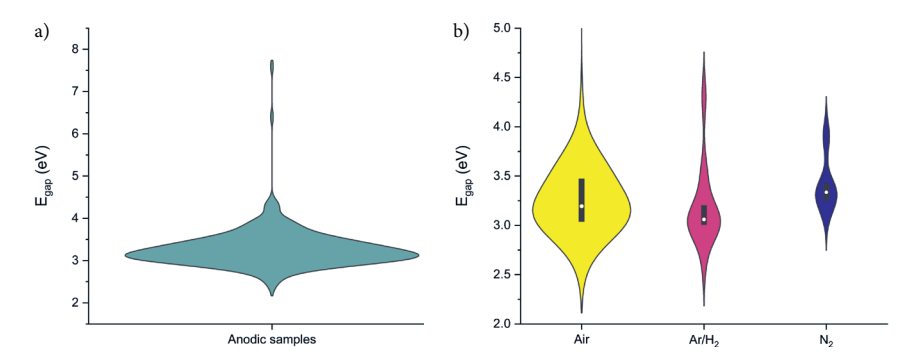


Fig. 21. a) Summary of $E_{\rm gap}$ values of all samples (not separated by heating temperature and atmosphere); b) Comparison of the optical absorption edge depending on the heating atmosphere, without considering the temperature distribution

the classic expected ${\rm TiO_2}$ E_{gap} values. Thus, annealing temperature and atmosphere are not the only influences on the optical properties of anodic titania; rather, synthesis parameters have a substantial influence.

3.1.3. Introduction of additives

As mentioned in the introduction and as we saw from the OCP and PCR data, the activity of NT coatings should still be improved, for example, by further shifting $E_{\rm gap}$ into the visible range and thus increasing the overall activity. The first impurity material is WO $_{\rm 3}$ particles. Further carbon NPs will be introduced, and the results will be investigated. NP introduction and composite coating synthesis classically is done in two steps with different methods; thus, to simplify the synthesis process, an inspired combination of anodization and deposition was devised; details are discussed further.

WO3 additives

A classic particle deposition method of WO₃ particles onto titania is electrophoretic (EPD), a method that has been approved in the literature. Electrophoretic deposition of particles is a classic method for the deposition of various particles, a detailed description can be found [76]. As the goal for synthesis optimization, EPD gave the inspiration to develop in situ additive introduction into anodic titania, i.e., combining electrophoresis with electrochemical anodization. Thus, these methods can be compared to evaluate the results. The in situ method used for the sample synthesis flowchart is shown in Fig. 22 a) and classic EPD in Fig. 22 b).

From the point of view of EPD, the electric field will induce a surface charge distribution on the additive particles, which will promote the movement of these particles toward the substrate, schematically shown in Fig. 23 a). In anodization,

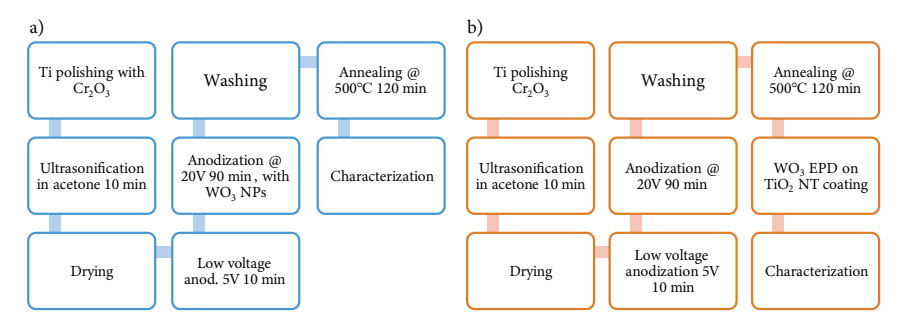


Fig. 22. Addition of WO₃ to NT samples. a) using developed in situ method – AW; b) using classic EPD method – EW

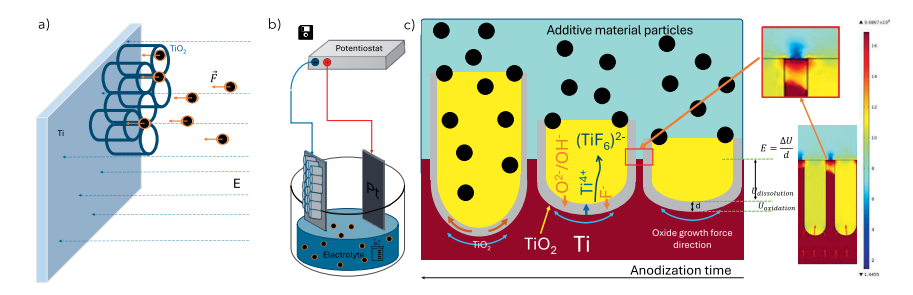


Fig. 23. Schematic representation of additive particles in situ introduction during anodization. a) schematic of the NT surface in electrolyte with particles; b) overall experimental setup analogous to EPD; c) representation of the electric field distribution, ion migration for tube growth, and particle injection during the anodization process. Electric field distribution adapted from [77]

the addition of particles to the electrolyte should not change the overall process because the particles themselves do not change the distribution of the electric field, a schematic depiction is shown in Fig. 23 b). Thus, combining EPD and anodization provides field distribution, as seen in Fig. 23 c), with the adapted distribution of the electric field and the effect of particles, an explanation of the proposed oxide growth model is provided. The model is based on the electric field distribution model found in literature [77], which is taken for the combined additive particle and tube electric field distribution over time exaggerated depiction in Fig. 23 c). It should be noted that in this case, the distribution of the electric field in the metal is not affected; the model considered NTs, which are more similar to aluminum anodized coating, i.e., primary growth into the base, whereas in the case of TiO₂, there is a combined process, both the depth of the pores into metal increases, and the oxide grows from the surface outwards, thus, the distribution of the electric field of the upper layers (electrolyte/oxide at the boundary surface) does not change; therefore additive particles can be implemented onto NT surface.

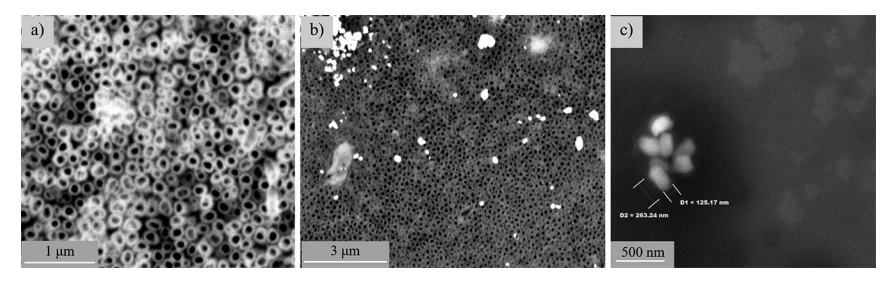


Fig. 24. SEM micrographs: a) TiO₂ tubular structure in an anodized sample; b) TiO₂ nanotube layer decorated with WO₃ particles; c) WO₃ particles with estimated size. Figure taken from Knoks et al. work [78]

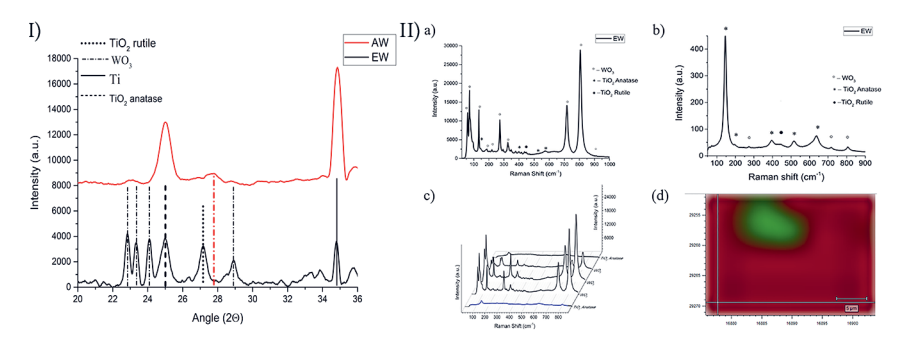


Fig. 25. I) XRD diffractograms of samples EW (black) and AW (red), pronounced Ti peaks coming from Ti base, pronounced WO₃ peaks at 2θ between 22° and 25° for monoclinic WO₃, TiO₂ anatase reflex around 25° and rutile reflex around 27°. II) Raman spectra of the EW sample, visible WO₃ particles on the surface. Figure taken from Knoks et al. work [78]

As a result of anodization, a TiO_2 NT coating is obtained, as seen in Fig. 24 a) and assessing the presence of WO₃ particles in the samples Fig. 24 b), WO₃ particles with average sizes around 125–250 nm are visible in Fig. 24 c). Microparticles resulting from the agglomeration of WO₃ particles are also visible on the TiO_2 surface.

The crystalline structure of EW and AW samples are shown in Fig. 25 I). Where the sample EW has the presence of WO₃ with pronounced monoclinic phase trio between $2\theta = 22^{\circ}$ and 25°, but the AW does not have a monoclinic WO₃ structure, which would indicate the phase transition that occurred during sample preparation, more precisely post-treatment annealing. The change is seen in the typical loss of 2θ peak intensities from 22° , 23° , and 24° . WO₃ crystallite sizes were estimated using Scherrer's equation (Patersons et al. [79]), using peak parameters $2\theta = 23^{\circ} - 40 \pm 5$ nm, while the size of TiO₂ crystallites is estimated at 17 ± 3 nm taken from $2\theta = 25^{\circ}$. It is well known that crystallite

size from XRD scattering using Scherrer's equation is only a qualitative indicator. The high-intensity Ti peak in the diffractograms originates from the Ti substrate. AT samples showed the standard anatase phase of TiO_2 , i.e., (101) peak at $2\theta = 25^\circ$. Similar results are gained from Raman spectroscopy seen in Fig. 25 II), where WO₃ vibrational modes are present in EW as particles seen in Fig. 25 d).

When evaluating photoactivity, it is the AW sample that shows a 55% and 36% decrease in OCP and PCR values, respectively; while the EW shows respectively 65% and 48% decrease compared to AT. However, it is worth noting that the AW sample showed a higher $N_{\rm D}$, and a faster charge separation compared to AT. It takes longer to reach the PCR and OCP plateau at the chosen illumination period, as can be seen, in Fig. 26 a) and b) with irradiation modulation. Not only does EW shows lower PCR values, but also a higher noise rate, which can be explained by WO_3/TiO_2 charge transfer and interfacial resistance. Additionally, AW has the fastest carrier separation dynamics, i.e., generated e^--h^+ are quickly separated, as we can see from a very rapid rise of PCR and quickly recombine when the light is turned off as seen by the quick drop. The decrease of AW parameters can be explained by the heat treatment of WO_3 , as shown in Fig. 26 c), where annealing the samples with WO_3 decreases their activity.

In the synthesis process, two methods of adding WO₃ were considered, in situ as additives of WO₃ particles to the electrolyte and after treatment in EPD. Using classical EPD and heating the samples results in a decrease in OCP and PCR and an increase in E_{gap}. Using EPD with excessive loading of WO₃ particles results in reduced OCP/PCR values. Despite the effect of heating, the introduction of in situ additives provides higher OCP and PCR values compared to the classical EPD method. The estimated charge carrier density shows, see the summary of results in Table 1, that adding WO₃ increases the amount of charge carriers and, in the case of AW, also increases the charge separation. Comparing the MB degradation shows that AW has the highest degradation coefficient. So, the developed method can be used to introduce additives.

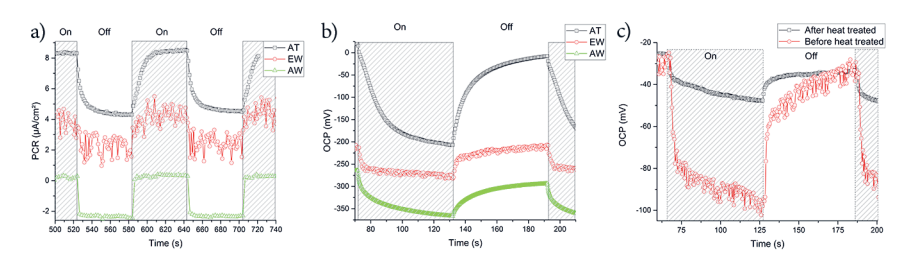


Fig. 26. OCP and PCR value dependence on the WO₃ introduction. a) PCR; b) OCP: Different WO₃ addition methods provides variation of results, pure TiO_2 showing the highest set of OCP and PCR values, yet different kinetics and N_D ; c) Comparison of OCP values with and without secondary annealing. After annealing the OCP value decreases. Figure taken from Knoks et al. work [78]

Table 1. The Summary of results in the case of OCP anodization is higher, PCR as well. The addition of WO₃ decreases the $E_{\rm gap}$ value when coated with EPD. ND increases by several orders of magnitude upon the addition of WO₃. Table taken from Knoks et al. work [78]

Sample	OCP, mV	PCR, µA · cm ⁻²	E _{gap} , eV	E _{Fb} , mV vs SCE	N_D , cm ⁻³	k, mol⋅min ⁻¹
AT	-222.6 ± 4.7	4.01 ± 0.20	3.11 ± 0.04	-1919.4 ± 0.2	$4.7\cdot10^{17}$	$-2.02 \cdot 10^{-5}$
EW	-80.5	2.07	2.86	-668.8	$1.6 \cdot 10^{21}$	$-2.06 \cdot 10^{-4}$
AW	-99.3	2.63	3.13	-799.3	$6.1 \cdot 10^{21}$	$-2.59 \cdot 10^{-4}$

Despite the E_{gap} shift into the visible wavelength range, we obtain lower OCP and PCR values. The optimal amount of WO₃ is a critical parameter for photocatalytic activity, as previously demonstrated. The transition of the generated charge carriers between these two materials, thus overcoming the barriers of the boundary surfaces, will directly depend on the ratio of the materials and the established contact, thus overcoming the Schottky barrier. If too much WO₃ is applied, much of the light is absorbed directly by the WO₃ and efficient separation of charge carriers does not occur. In the currently accepted model, the generated e⁻-h⁺ pairs pass through the boundary surface, i.e., holes from the valence band of WO₃ to the valence band of TiO₂ and electrons from the conduction band of TiO2 to the conduction band of WO3. It is known that incorporating tungsten as a defect into TiO₂ structures effectively reduces E_{gap}. In the case of NT coating, the process is similar, in addition a better e⁻ conduction is formed due to nanotubes, which was confirmed by increased kinetics. Thus, alternative materials should be sought after without the negative effects of annealing.

Introduction of carbon material additive

While looking for alternative ways to further increase photocatalytic activity carbon materials pose an attractive option. In this work for inorganic based electrolyte three carbon materials were introduced. AFM was used to evaluate the obtained particles, while SEM and structural investigation, carried out by Raman and XRD, was done after the introduction into titania. For AFM measurements particle dispersion was diluted with deionized water roughly ten times, then using precision spray gun deposited on monocrystalline wafers. Size of H particles, obtained in hydrothermal synthesis, was estimated around 2.1 nm, as seen in Fig. 27 a) and b), the width up to 53.1 nm, as can be seen in Fig. 27 c), although the width indicates agglomeration during substrate drying. AFM of exfoliated few-layer graphene (G) particles shows similar results with a particle size of around 2.9 nm and a width of 50.8 nm, the overall analysis of the results is analogous to the case of H, results shown in Fig. 28. AFM images of commercial graphene quantum dots with green luminescence (Q), as seen in Fig. 29, show a height of 6.6 nm and a width of 31 nm as seen in c). This indicates

a small particle size, as expected for multilayer graphene particles and their agglomeration. Therefore, the sizes of the examined particles are comparable.

It is worth noting that there are many examples in the literature where composite material combinations are attempted, these particles also can be simultaneous deposition during anodization. Therefore, the selected *in situ* additive introduction method model can be validated with different types of particles. By adding carbon materials to an inorganic electrolyte, we see that the absorption edge also changes, i.e., there is a shift depending on the type and amount of carbon additive, as can be seen Fig. 30. We can observe that $E_{\rm gap}$ shifts from the classical position at 3.2 eV for anatase or 3.0 eV for rutile to about 2.9 eV. The addition of Q gives a similar result in reducing $E_{\rm gap}$, i.e., moving it deeper into the visible range.

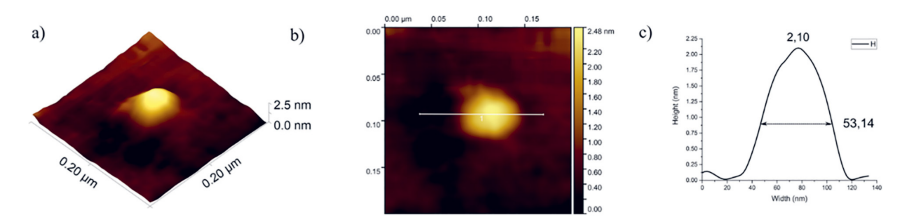


Fig. 27. AFM examination of particle H: a) overall appearance in 3D; b) 2D image with selected profile; c) particle profile. Figure taken from Knoks et al. work [80]

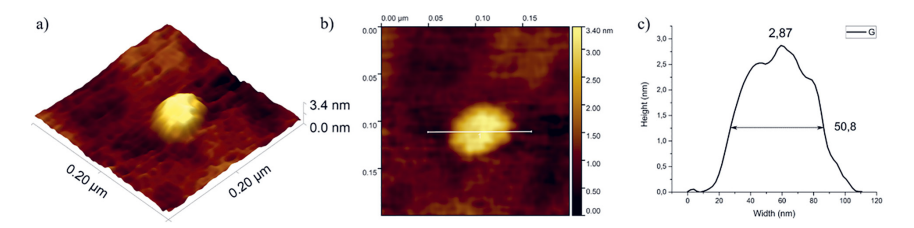


Fig. 28. AFM examination of particle G: a) overall appearance in 3D; b) 2D image with selected profile; c) particle profile. Figure taken from Knoks et al. work [80]

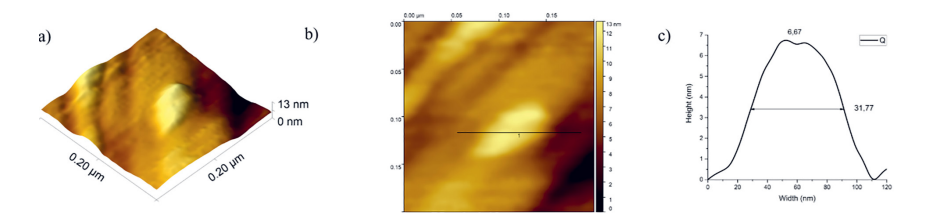


Fig. 29. AFM examination of Q particle: a) overall view in 3D; b) 2D image with selected profile; c) particle profile. Figure taken from Knoks et al. work [80]

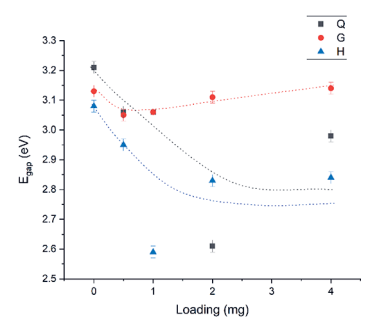


Fig. 30. Effect of carbon admixtures on $E_{\rm gap}$ position of samples, normalized values against pure sample. The addition of reduced graphene flakes initially decreases and then increases the absorption edge, the commercial material generally decreases the position of the absorption edge, and the hydrothermally obtained C material also decreases the $E_{\rm gap}$ value. Figure taken from Knoks et al. work [80]

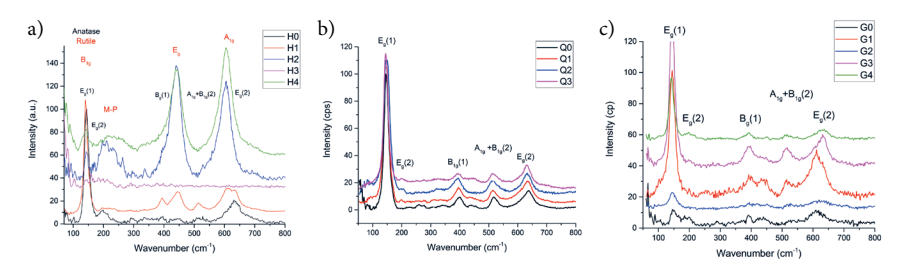


Fig. 31. Raman spectra of a TiO_2 film obtained in an inorganic electrolyte with the introduction of in situ additives, the allotropic phase changes depending on the type and amount of additive material. a) The H series show a change from anatase at a low amount of additives to apparently rutile/brookite at a higher amount of additives; b) Q remains an anatase phase throughout the series; c) Anatase also remains primarily phase in the case of G. Figure taken from Knoks et al. work [80]

When performing a structural analysis of the series with the introduction of Q, G, H, we see that depending on the type and quantity of the additives, the structural properties change, i.e., phase ratio as well as other related parameters. Let's remember that the series of samples were heated under the same conditions, therefore in case the additive materials do not affect the phase transitions, all samples should be in the same polytropic phase. Here we see the structural changes in the phase composition, which is not described in the literature.

Assessing the phase change of the structures of these samples are also visible by with Raman spectroscopy measurements, which are visible in Fig. 31. While Fig. 31 a) structure appears to be a change from A to R/B mixture due to H additive, b) and c), respectively, Q and G series, primarily show an anatase

phase. Changes in the structure of the H series allow us to compare the Raman spectra of brookite, which is not an expected result. It is known that additives can cause changes in position and shape/width of vibrational modes, as described by Ceballos-Chuc et al. where anatase nanocrystals with 15% brookite admixture show the asymmetric mode formed from the anatase Eg and brookite Alg modes while at the same time the brookite Blg and B3g modes introduce an extension [81].

The crystalline structure of all samples with Q is also anatase phase throughout the coating, including visible Ti Bragg peaks coming from substrate foil. However, these samples also show R(101), which may be a thermal oxide or an A-R transformation has occurred. Looking at the A/R ratio, we can see that compared to pure as anodized samples, the introduction of additives changes the proportion of A, indicating a decrease. In the case of the Q series, the amount of rutile appears to increase slightly. On the other hand, for the samples with G additives, a directly opposite result, the amount of additive increases the intensity and proportion of A. It would be expected to some extent that the presence of carbon is able to reduce TiO₂ more. So, for samples G and Q, the XRD plots are as expected, see Fig. 32 a), b) and c), while additional Bragg peaks appear for the H series, the prominence of which cannot be observed in the G and Q samples, as can be seen from the respective comparison Fig. 32 d). The Bragg peaks can be attributed to the brookite form of TiO₂, which has not been observed so far empirically or in the literature for an anodic coating of titanium oxide nanotubes. Moreover, that corresponds to Raman investigation results.

Evaluating the A/R/B ratios of the samples as shown in Fig. 33, in the G series, additive contributes to an increase in the proportion of anatase Fig. 33 a), the Q-series additives seem to promote a small development of rutile as seen by changes of the relative intensity ratio seen in Fig. 33 b). On the other hand, with an increase in the amount of H additives promotes the development of brookite and rutile phases, as seen in Fig. 33 c).

From the structural analysis we can see that the crystalline structure changes for all samples, it is worth noting that the crystallite sizes of the samples also change. Changes in crystallite size with decreasing amount of A are expected because the anatase-rutile or brookite phase transition involves breaking and re-forming of interatomic bonds, followed by reorientation and reduction of the unit cell. As well as rutile crystallites at the considered temperatures primarily grow from/on grain boundaries. For example, if phase transitions are viewed in the context of NPs, as the proposed model is based on nanoparticle interface contact points as transition nucleation sites [82]. Kandiel et al. synthesized NPs with different A/R/B compositions and ratios in both pure and mixed form using urea as a precursor. They note that each phase is thermodynamically stable at different crystallite sizes A below 11 nm, B between 11 and 35 nm, and R above 35 nm, which would indicate that crystallite size could be indicative

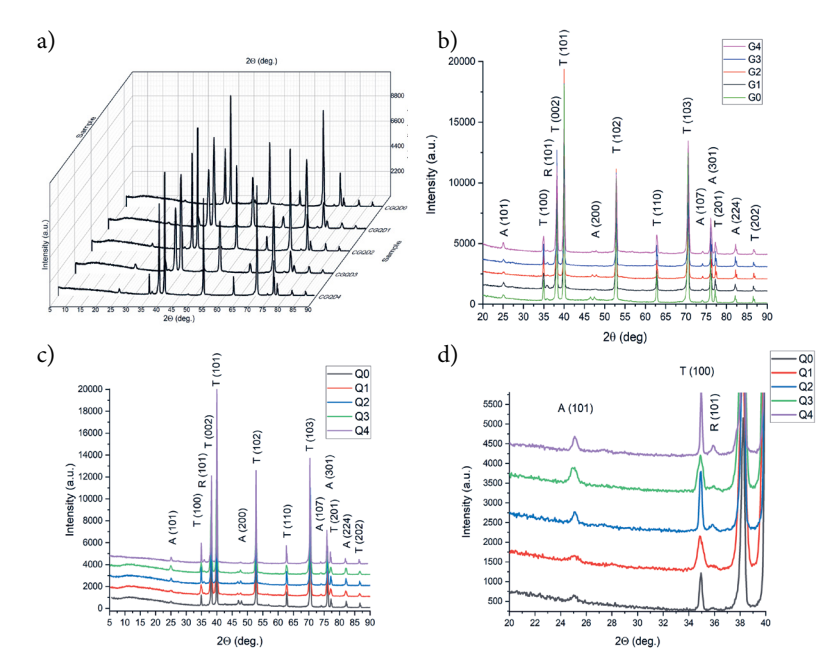


Fig. 32. XRD diffractograms of TiO₂ samples with Q, G and H additives. a) Spatial plots of XRD with Q; b) XRD of G-series; c) XRD of Q-series; d) XRD diffractograms of H, we see a mixture of A with brookite and rutile. Figure taken from Knoks et al. work [80]

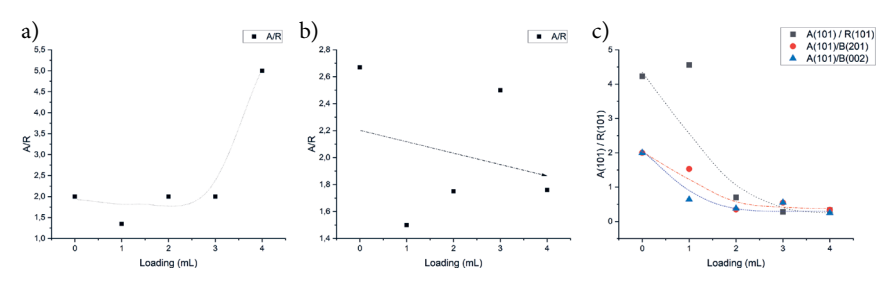


Fig. 33. A/R ratio comparison from XRD Bragg peak intensities. a) G – series, an increase in the amount of CNP promotes an increase in the proportion of A phase; b) Q – series, an increase in the amount of CNP promotes the proportion of the R phase; c) H series, CNP additives promotes B and R phase development

of phase identification. It is also noteworthy that the phase transitions usually occur from A to R and from B to R [82].

Carbon is a strongly reducing additive, especially in combination with a reducing atmosphere which creates oxygen vacancies, a defect type, and remembering that the anatase – rutile transformation includes bond reorientation, we can explain the increased amount of rutile/brookite along with the increase in the amount of additive material due to the reducing nature. The presence of carbon as a reducing agent is also found in the literature [83], but it should be noted that in the mentioned works C is a dopant and the accepted mechanism foresees the formation of CO_2 in the process. On the other hand, in the case of adding particles and plates, no structural changes have been observed in the literature, even when synthesizing composite nanoparticles. The presence of interatomic Ti^{4+} and F^+ oxygen vacancy defects affect the expansion of the crystal lattice, whereas the electrostatic interaction between interatomic Ti^{4+} and O^{2-} and oxygen vacancy defects causes a change in the lattice concentration in undoped TiO_2 nanostructures. The redshift for the E_g and A_{1g} modes is due to phonon trapping and again to oxygen vacancy defects, which respectively cause the unit cell to increase due to O^* [71; 84].

The introduction of carbon additives affects the crystalline structure and lattice parameters, thereby affecting the position of the XRD Bragg peaks, which is also reflected in the shift of the Raman modes. Some samples undergo a complete phase transformation from anatase to another polytropic form; with phase change directly depending on the type of additive CNP. Specifically, sample series H clearly shows an increase in the proportion of rutile and brookite phases. In contrast, G and Q series, no such transition is observed either in Raman or XRD results. This can be attributed to the higher defect density on the surface of hydrothermally obtained carbon particles, which have a greater reducing power due to unpaired sp² bonds. In combination with a reducing atmosphere, which performs a similar function, i.e., creates additional oxygen defects and thus, by increasing the amount of broken bonds, it contributes to the total amount of defects, which, in turn, contributes to the phase transition from anatase to rutile/brookite. A schematic representation of the proposed mechanism can be seen Fig. 34.

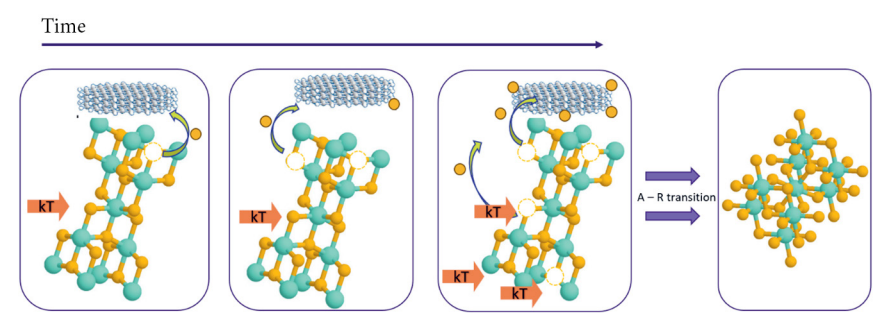


Fig. 34. Proposed A-R/B phase transition with the presence of CNPs annealed in a reducing atmosphere. Figure taken from Knoks et al. work [80]

For Q particles from the Raman shift data, we see the D mode indicating armchair edges [85] indicating a passivated surface, i.e., Q has fewer reducing centers and thus a smaller contribution to the formation of oxygen vacancy defects in the composite TiO_2 coating, which leads to a higher proportion of anatase in the entire range of additives considered. A similar explanation can be applied to the G samples, the shape and condition of the edges are with lower number of defects. Therefore, the addition of G does not contribute to the formation of oxygen vacancies and thus, phase transition.

Two other noteworthy things, first, anodic coatings of TiO₂ nanotubes in the brookite phase were not observed in the reviewed literature. Second, the H-samples show a significant presence of R(110), as seen in Fig. 32 d) in addition to other B peaks. R(110) has been ascribed to the thermal rutile oxide formed on the NT and metal interface. Despite the fact that the literature notes that this R(110) is formed only in the presence of air (oxygen) as a result of Ti oxidation. Considering that the heating takes place in a reducing oxygen-free environment, further research and analysis of this process is necessary.

For photocatalytic activity, investigation of the G, Q, and H series shows changes in OCP and PCR depending on the type and amount of additives, results are depicted in Fig. 35. By introducing the carbon material into the inorganic electrolyte, we see that while for G the OCP is decreasing Fig. 35 a), the exact opposite effect is seen for both the H and Q series, an increase in the OCP values as seen in Fig. 35 b) and c). It is similar with the PCR values, at least for H, but both G and Q give an initial decrease, although in the case of Q a subsequent increase is also observed as the amount of additives increases.

The summary of degradation coefficients can be seen in Fig. 36. The addition of G reduces the photocatalytic activity of TiO_2 . Although no clearly pronounced trend can be observed, all obtained values are lower compared to as anodized TiO_2 . The addition of H increases the photocatalytic activity as the additive amount increases, while the addition of commercial graphene quantum dots increases the activity with a small added amount, but the activity decreases as the amount continues to increase. These results are in agreement with the previously described and other photophysical and electrochemical properties.

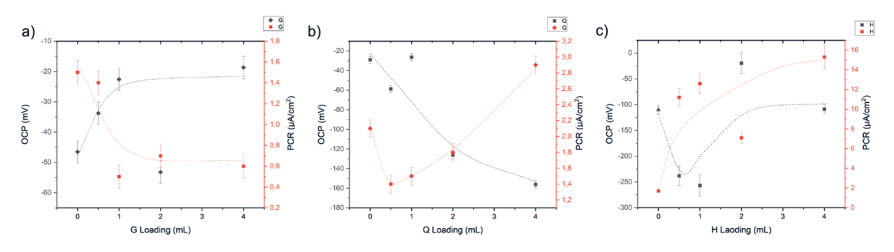


Fig. 35. OCP and PCR dependence on the additive CNP amounts. a) G; b) Q; c) H

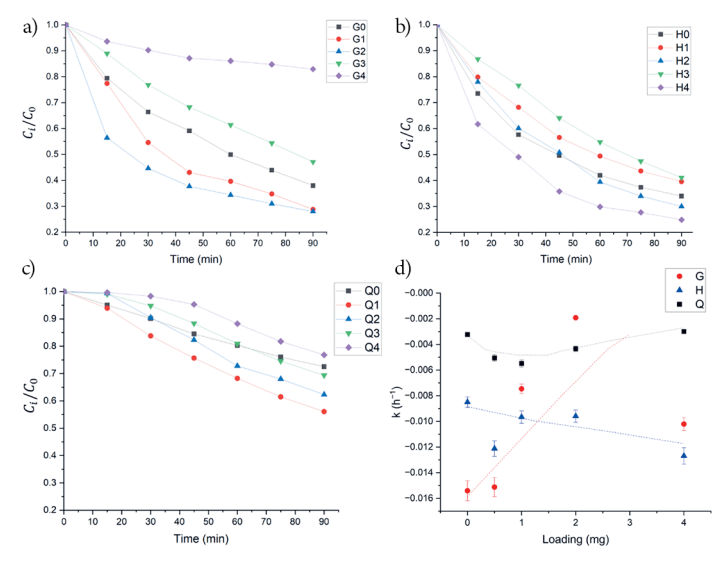


Fig. 36. MB C_i/C_0 decrease in time depending on the amount of CNP additives a) G; b) H; c) Q; d) degradation coefficient dependency on the amount of G (\bullet), H (\triangle), Q (\blacksquare). Figure taken from Knoks et al. work [80]

An overall comparison of parameters can be seen in Table 2, the Q material reduces $E_{\rm gap}$ but increases the $E_{\rm Fb}$ while increasing OCP and PCR at higher concentrations. The biggest changes are observed for H series samples where OCP and PCR values increase significantly with the addition of H, and $E_{\rm gap}$ decreases and $N_{\rm D}$ increases, which can be attributed to increasing the proportion of the brookite phase in samples.

3.2. NT coatings synthesized in an organic electrolyte

The coatings obtained in the organic electrolyte are anodized twice, this is due to the fact that the first anodization is obtained in the form of flattened oriented tubes, as can be seen in Fig. 37 a). Such tube growth is very briefly noted in the literature as nanograss or similar, but not much emphasis is placed on it [86], although there are also works in which it is accepted as the norm [87]. Currently, the explanation is that chemical etching is superior at larger anodization times and distances from the Ti base, the walls thin out until the hydrodynamic pressure flattens them, but the overall electric field distribution on the base surface promotes the formation of row structures. We can see that clearly in Fig. 37 b), different phases of NT development 1. self-oriented NT coating 2. interface between oriented and flattened tubes 3. flattened and collapsed tubes. Analogously, in a macroscopic manifestation, the stalks in

Table 2. Summary of sample parameters obtained in inorganic electrolyte depending on the amount and type of additives. Table taken from Knoks et al. work [80]

Added material	Sample	OCP, mV	PCR, μA·cm ⁻²	E _{gap} , eV	E _{Fb} , mV	N _D 10 ¹⁷ , cm ⁻³
	Q0	-29.1 ± 4.7	2.1 ± 0.2	3.21 ± 0.04	-908.0 ± 0.2	15.4
	Q1	-58.7	1.4	3.06	-1004.6	17.8
Q	Q2	-26.3	1.5	3.06	-1034.0	18.2
	Q3	-126.1	1.8	2.61	-1015.0	28.2
	Q4	-156.1	2.9	2.98	-1036.0	27.8
	G0	-46.5	1.5	3.13	-942.5	97.8
	G1	-33.8	1.4	3.05	-1011.1	21.5
G	G2	-22.6	0.5	3.06	-959.2	3.95
	G3	-53.2	0.7	3.11	-947.9	4.99
	G4	-18.7	0.6	3.14	-704.2	68.5
Н	H0	-109.9	1.7	3.08	-725.0	9.17
	H1	-238.2	11.2	2.95	-988.5	1.97
	H2	-256.8	12.6	2.59	-1059.8	30.1
	Н3	-19.5	7.1	2.83	-816.2	126.0
	H4	-108.7	15.3	2.84	-1060.0	133.0

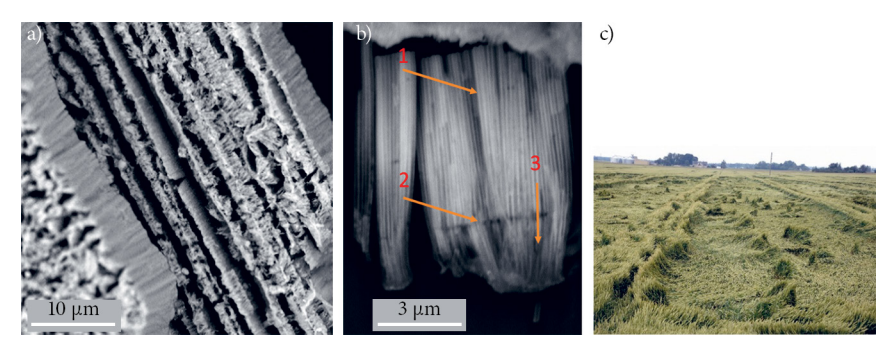


Fig. 37. NT coating in single step anodization in organic electrolyte. a) SEM micrographs of coating with flattened surface, cross-sectional view; b) SEM micrograph of NT coating profile with distinctly visible 1 self-oriented NTs, 2 boundary surface where the reduction of tube thicknesses begins, 3 flattened walls; c) Photography of wheat fields flattened after rain due to the collapse of the stems. A coating with a flattened surface is obtained in the simple anodization of an organic electrolyte is analogous to macroscopic natural phenomenon

the wheat fields collapse and form regular flattened structures Fig. 37 c). Overall, this is detrimental to activity, therefore, double anodization is always used with the peel-off method by removing the first anodized layer.

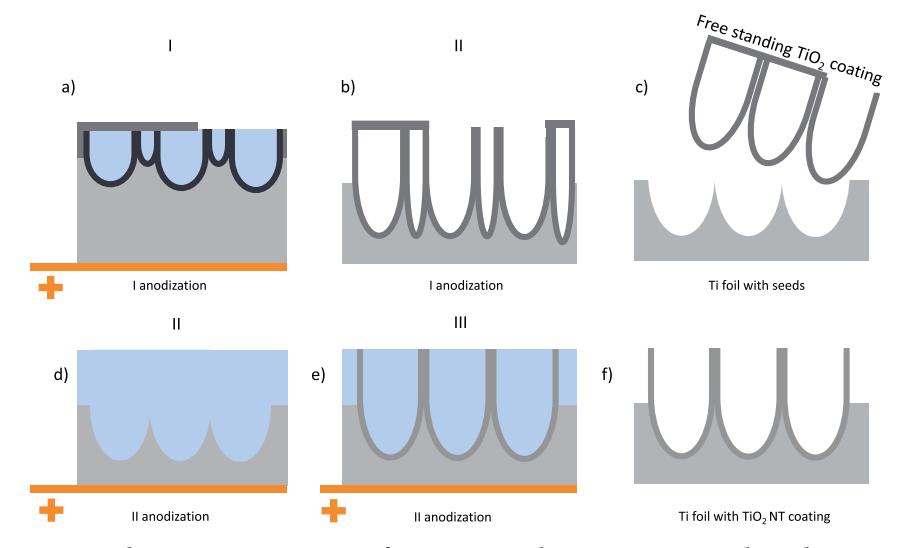


Fig. 38. Schematic representation of two-time anodization in organic electrolyte. a) first anodization; b) NT coating with dense oxide and flattened tubes on top; c) peel off method to leave NT seed imprint; d) second anodization; e) uniform NT coating growth; f) final NT coating with open ends

Double anodization can be described with a schematic representation, as seen in Fig. 38. In connection with the described model where oxide tubes grow on the metal/oxide interface Fig. 38 a), then gradually going into the metal foil and raising the oxide layer upwards Fig. 38 b). Therefore, when performing the first anodization, it is possible to create tube sees in the base, as discussed previously for inorganic anodization and shown Fig. 17. When the oxide layer is removed, as shown Fig. 38 c) and d), with peel-off method, secondary anodization is done Fig. 38 e). Therefore, the double anodization results in a coating of open tubes Fig. 38 f).

3.2.1. Effect of NT coating thickness on photophysical parameters

Literature indicates that the length of NT affects photoelectrochemical properties, it was necessary to evaluate the effect of length on OCP, PCR and other electrochemical parameters. For as-grown NTs in an inorganic electrolyte, we saw that increasing the anodization time (and thus the coating thickness, or the length of the tubes) changes the photoelectrochemical properties proportionally to the length, as well as the proportion of anatase increases proportionally. Suppose that by increasing the anodization time we get a larger increase in COP, PCR, and other parameters of photocatalytic activity proportional to the length/anodization time. In this case, the first anodization round was performed for 60 min at 60 V.

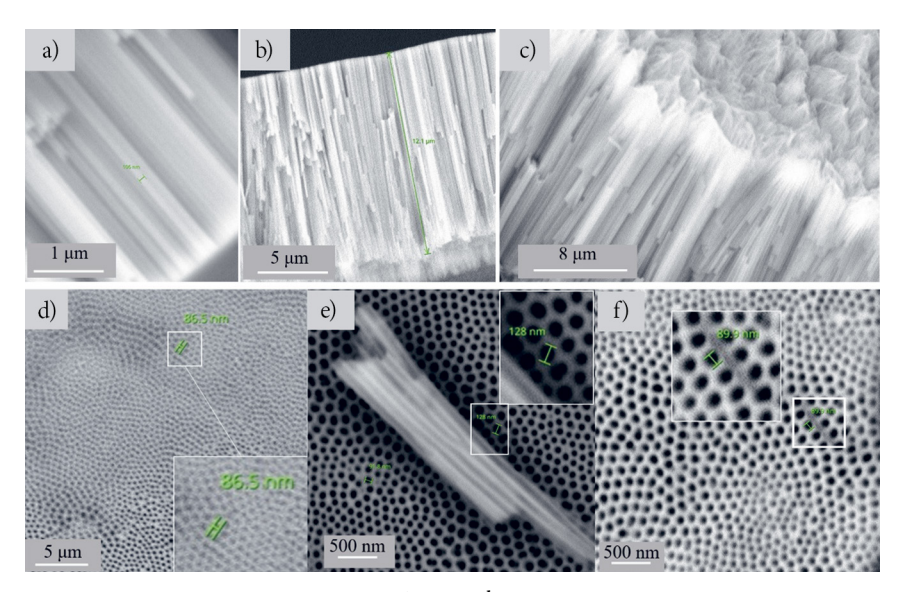


Fig. 39. SEM micrographs, result of 1st and 2nd anodization of TiO₂NT obtained in organic electrolyte. After first anodization a) NT side view; b) NT profile; c) NT profile for sample 3. after second anodization; d) 20 min anodized; e) 40 min anodized; f) 60 min anodized sample

SEM images of the discussed defective layer are shown Fig. 39 a), b), and c) or analogous to Fig. 37. Then it is removed, Fig. 38, by applying a layer of hot glue and allowing it to harden, this layer can be removed without damaging the Ti base. It is worth noting that such a removal method, no matter how simple it is, was not found in the reviewed literature and allows to simplify the obtaining of high-quality NT layers. Analogous to the application of the "adhesive tape" method for obtaining graphene [88] a seemingly simple but effective way to clean the top layer and get a seed layer system. On the other hand, the methods adopted in the literature, such as sonification and polarization, did not give fast and high-quality film removal results.

After the second anodization, which is carried out for 20, 40, and 60 min, a coating of the open tube system is obtained, see respectively d), e), and f) in Fig. 39, result in the same type of surface area and expected better photoelectrochemical properties. Looking at the SEM micrographs of these surfaces, we see that very similar tube coatings are obtained, which is expected from the same anodization voltage, electrolyte, and temperature, where the average tube diameter is around 90 nm.

NT parameters are summarized in Table 3, we can see that the amount of anatase increases similarly to the inorganic electrolyte samples, PCR and OCP values increase, at the same time the onset potential increases while E_{Fb}

 $\it Table~3.$ Structural and photophysical parameters of samples obtained in organic electrolyte

	Length, µm	A/R	PCR, μA·cm ⁻²	OCP, mV	E _{onset} , mV vs SCE	E _{Fb} , mV vs SCE	N _D , cm ⁻³
20min	2.82 ± 0.25	9.3	13.5 ± 0.2	-57.9 ± 4.7	-819.0 ± 0.2	-1147.0 ± 0.2	7.91 · 10 ¹⁶
40min	3.57	15.4	20.4	-80.9	-857.0	-1163.0	1.88 · 10 ¹⁶
60min	4.1	12.9	51.7	-112.9	-891.0	-545.0	4.48 · 10 ¹⁷

decreases. All parameters seem to improve when reaching 60 min of anodization time. On the other hand, by increasing the time even more NT coatings start to peel off depending on the composition of the electrolyte, therefore a second anodization round of 60 min is used from now on.

3.2.2. Carbon particle additives in anodic coatings synthesized in an organic electrolyte

In the inorganic electrolyte we saw that it is possible to use C-based additives, in the organic electrolyte two materials with catalytic potential were chosen: carbon particles doped with platinum, denoted as CP, and self-synthesized reduced exfoliated graphene particles doped with nitrogen, denoted NC. Synthesis was carried out in two anodization times with the removal of the first NT layer, anodization performed at 60 V for 60 minutes, and in the second round, similarly, 60 V and 60 minutes in a new electrolyte, CP or NC additives were added in the following concentrations 0.0; 0.001; 0.002; 0.01; 0.02 and 0.08 wt%.

When taking SEM micrographs, we can see that without the addition of additives, a coating of nanotubes with an average tube diameter of 80 nm is obtained; there is also a slight flattening of individual tubes, as if they had coincided on the common NT surface, as can be seen in Fig. 40 a) and b) NC1 additive allows NT with thick walls.

At the maximum amount of additives, 0.08 wt%, we can see that the shape of the tubes is still preserved, but the amount of flattened tubes due to bursting has increased Fig. 40 c) and d), i.e., it is visible in which places the pipes have exceeded the growth limit, where chemical dissolution is dominant and the thickness of the walls decreases, which results in the overpowering of the hydrodynamic pressure and the pipes breaking. In the upper layer of tubes, the walls are thinner in comparison to NC1.

On the other hand, the series of samples with CP additives show different results. Sample CP1, with 0 CP NPs, shows a smooth tube surface, the tubes are well oriented, with no obvious notches/waves on the walls, as seen in Fig. 41. Which indicates optimized electrolyte content and could indicate potential activity.

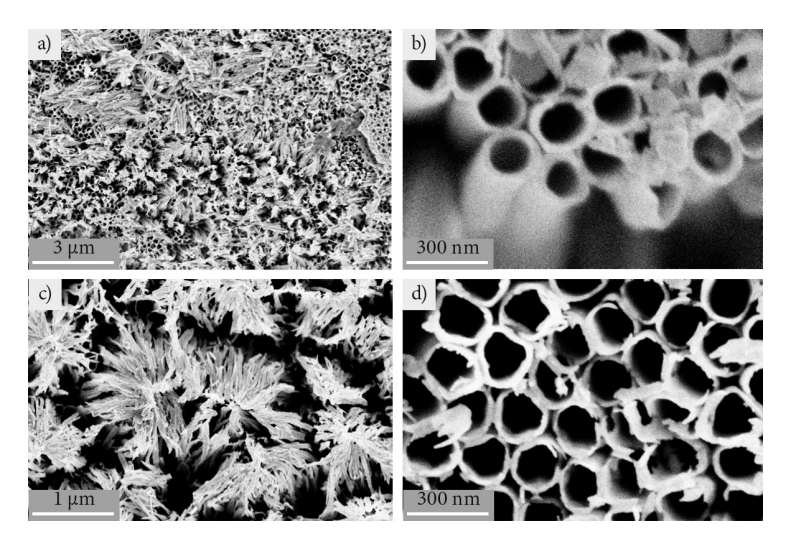


Fig. 40. SEM micrographs a) NC1 general view of broken NTs; b) NC1 in higher magnification we can clearly see tubes with thick walls; c) NC sample with 0.08 wt% NC admixture: flattened and contracted NTs can be seen centrally; d) tubes grown at the bottom have a distinct cylindrical shape and electrolyte closer to thin walls

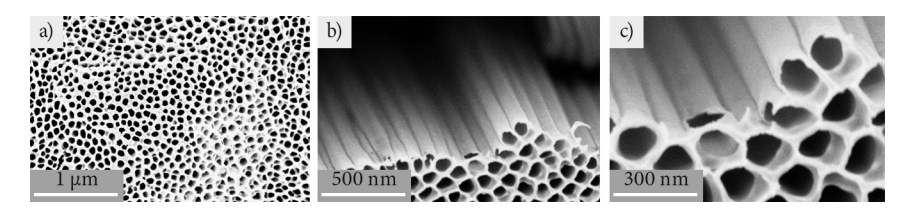


Fig. 41. SEM micrographs. The first sample of the CP1 sample series without additives. a) NT coating with open pipe surfaces; b) side view of the pipe walls; c) we can see the additional splitting of the pipe walls closer to the coating surface

With the highest selected concentration of additives, 0.08wt%, SEM images are shown in Fig. 42, the synthesized coating is uniform, NTs are well defined, though there are additional particles on the coating surface, as seen in Fig. 42 b). NTs have relatively thick walls, which are still not different from other wall thicknesses in the CP series. The upper layer, as in other samples, is not as pronounced as in other samples, the tube system goes to the surface. It is worth noting that both the top layer and top particles are porous, as can be seen in the higher magnification Fig. 42 c) and d). Elemental analysis revealed that these growths are also TiO₂.

Both CP and NC samples show distinct tube morphologies with different types of top layer. NC wall thickness has decreased while the oxide continues to grow in length, leading to flattened or broken walls on the coating surface.

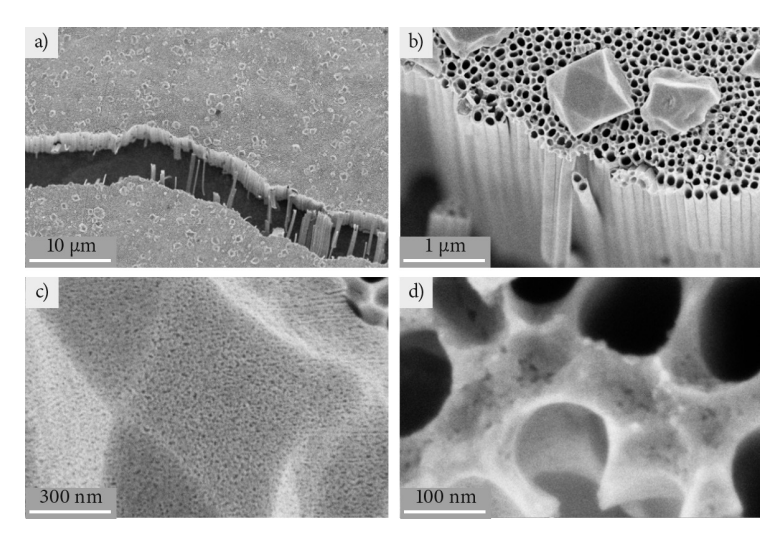


Fig. 42. SEM images of sample CP6 a) NT coating is torn during the heating and drying process; b) visible NT with pipe system and crystalline particles on the surface; c) particles on the surface are porous; d) the walls of the upper NT coating are also porous

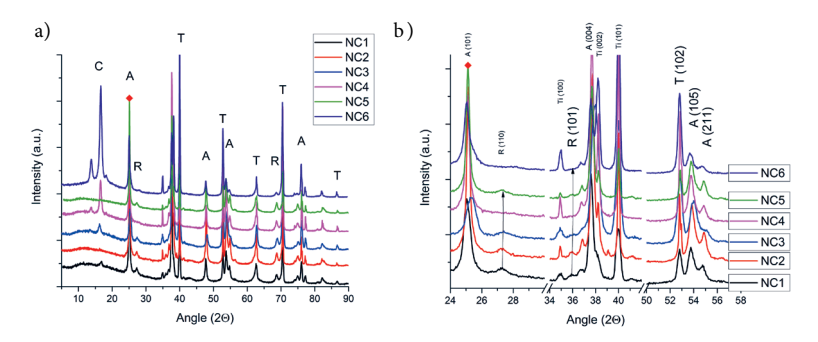


Fig. 43. XRD diffractograms of TiO_2 samples depending on the amount of NC additives. a) Overview with an increase in the C Bragg peaks as the amount of additives increases; b) XRD graph with an emphasis on the decrease of the R(110) as the amount of NC increases. The coverage of the samples is expressed primarily in the A phase. Figure adapted from Knoks et al. work [89]

In the case of CP, the collapse of such walls is not observed, but TiO₂ particles are visible on the surface of the coating in a large additive case.

XRD data clearly show, firstly, that the coating obtained is primarily in the form of anatase, as can be seen Fig. 43 a), with intense A (101) peak at $2\theta = 25^{\circ}$. At the same time Fig. 43 b) it can be seen that at none to low NC amounts, there

are rutile peaks at $2\theta = 36^\circ$ corresponding to rutile (101), this is clearly visible in NC1. Also, there is the presence of the thermal oxide R(110), which decreases with increasing NC amounts, as seen from $2\theta = 27^\circ$ decrease in intensity. Raman spectra show a shift of the carbon modes but no presence of rutile, while XRD anatase (101) 2θ shows a shift indicating a lattice change. Therefore, even a small amount of NC additives in the electrolyte contributes to a different composition of phases. Increasing the amount of NC leads to a more pronounced anatase composition.

What is unclear is how the thermal oxide can form, if it is a thermal oxide and not the result of the anatase rutile transformation, since it must be formed by heating TiO₂ in an air atmosphere, where the possible explanation is that the oxygen, which is necessary for the formation of rutile, is "taken" from the anatase, i.e., from the existing neighboring TiO₂. The literature reviewed does not answer this question. Let's remember that we saw a phase transition as a result of the addition of H particles in the NT coating obtained in an inorganic electrolyte with additives of carbon materials, i.e., some amount of brookite was obtained. On the other hand, the addition of NC promoted the formation of an anatase phase similar to the G series in inorganic electrolyte. In this case, both NC and G materials were obtained as a result of exfoliation.

In contrast, the addition of CP not only promotes the formation of the rutile phase but also the formation of the brookite phase, as can be seen Fig. 44 a); it clearly shows that the addition of CP particles during the synthesis process changes the obtained structure along with the amount of added CP similar to what was found in the case of H additives in the inorganic electrolyte. On the other hand Fig. 44 b) shows an appearance and increase of R(110) despite the fact that the samples were heated under nitrogen.

Degradation coefficient was determined and compared to as-anodized samples, i.e., 0.0 additives. The changes in the obtained degradation coefficient compared to the pure sample can be viewed Fig. 45. The addition of CP NPs increases the photocatalytic activity as seen by the increase in k_i/k_0 , on the other hand, the addition of NC decreases the k values, which could indicate less charge carriers reaching the MB molecules and more recombination, but as we can see in Table 4, PCR increases with the addition of NC. On the other hand, the onset potential increases in the cathodic direction, further reducing the $N_{\rm D}$, which indicates less available charge that could be involved in the reduction reactions, indicating that the NCs act as electron capture centers/electron concentration points, but do not undergo MB adsorption on them, resulting in decolorization. speed decreases.

The addition of carbon additives to TiO_2 nanotube coatings affects not only their photocatalytic activity but also crystalline structure, with varying results depending on the type of additive. CP additives enhance photocatalytic activity, likely due to an increase in charge carrier density (N_D) and changes in structure, similar to anodic TiO_2 synthesized in inorganic electrolytes shown in this thesis. This supports the idea that an increase in brookite phase content improves photocatalytic activity, as brookite outperforms anatase and rutile in this regard.

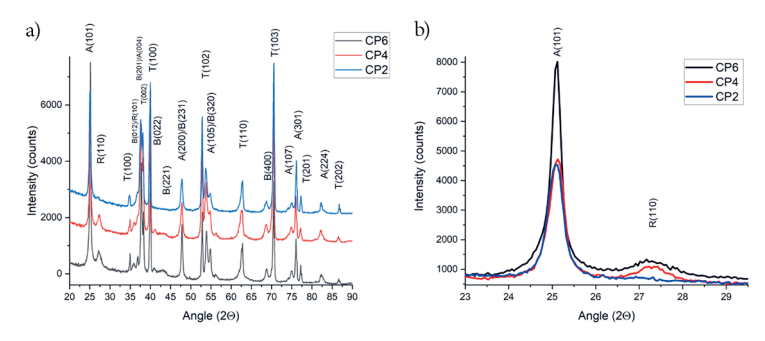


Fig. 44. XRD diffractograms of TiO₂ samples depending on the amount of CP: a) Overview, presence of A/R/B phase mixture is visible; b) Increase of relative intensity of R(110) with increased CP amounts. Figure adapted from Knoks et al. work [89].

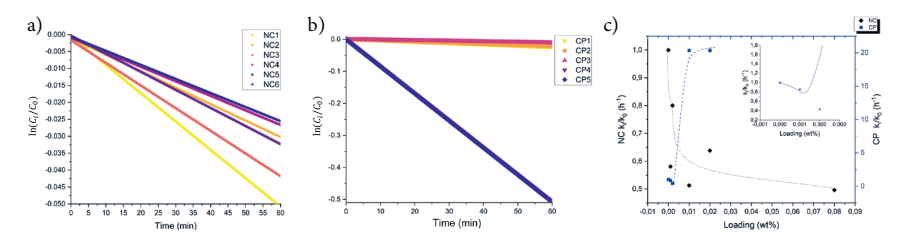


Fig. 45. Photocatalytic activity of TiO₂ samples with NC and CP. a) degradation coefficient k dependence no NC amount; b) degradation coefficient k dependence no NC amount; c) relative k changes with respect to the pristine TiO₂ sample. Blue square CP, Black diamond NC. MB degradation increases for CP and decreases for NC samples. Figure taken from Knoks et al. work [89]

Table 4. CP and NC result summary. PCR relative change vs pristine TiO_2 , onset potential values and MB degradation coefficient. An increase in CP increases k, and decreases E_{onset} on the other hand NC additives decrease k and increase PCR as well as E_{onset} . Table taken from Knoks et al. work [89]

Sample	PCR _i / PCR ₀	E _{onset} , V vs SCE	k, mol·min⁻¹	Sample	PCR _i /PCR ₀	E _{onset} , V vs SCE	k, mol·min⁻¹
CP1	1	-0.86 ± 0.05	$-4.16 \cdot 10^{-4}$	NC1	1	-0.70 ± 0.05	$-8.36 \cdot 10^{-4}$
CP2	0.42	-1.00	$-3.57 \cdot 10^{-4}$	NC2	4.69	-0.80	$-4.86\cdot10^{-4}$
CP3	0.75	-0.81	$-1.79 \cdot 10^{-4}$	NC3	1.56	-0.85	$-6.69 \cdot 10^{-4}$
CP4	0.59	-0.61	$-8.46 \cdot 10^{-3}$	NC4	1.17	-0.92	$-4.29\cdot10^{-4}$
CP5	0.22	-0.69	$-8.46 \cdot 10^{-3}$	NC5	1.91	-0.87	$-5.34 \cdot 10^{-4}$
CP6	0.14	-0.57	$-8.82 \cdot 10^{-3}$	NC6	_	_	$-4.15\cdot10^{-4}$

CP additives also increase the NT surface area, enhancing photocatalytic performance. In contrast, NC additives decrease activity, likely due to surface degradation, which reduces charge carrier transfer and increases recombination.

In summary, the composite synthesis method for TiO₂ coatings, incorporating various carbon materials in organic electrolytes, demonstrates changes in structure and phase composition. Key findings include:

1. NC Additives:

- a) OCP and PCR change in proportion to the additive amount.
- b) Shift in onset potential to more negative values.
- c) Shift in E_{Fb} to more positive values.
- d) Decreased degradation coefficient due to morphological changes.

2. CP Additives:

- a) Promotes brookite phase formation.
- b) Decreases OCP and PCR values compared to as-anodized samples.
- c) Shifts onset potential to more positive values.
- d) Increases N_D, providing more available charge carriers.
- e) Enhances MB photocatalytic degradation.

4. CONCLUSIONS

In this work, variations of titanium dioxide nanostructured coatings for photocatalytic property improvements were investigated. Anodic titania was obtained with variation in synthesis parameters, and its influence on photocatalytic properties was investigated. It was found that the synthesis parameters are of substantial importance and contribute to the obtainable crystalline structure and photocatalytic properties. In the literature, there is no consensus on the temperature of ${\rm TiO_2}$ phase transitions and their dependence on synthesis methods, which is demonstrated in this work. Therefore, the choice of synthesis and processing parameters must be based on the final intended application. To further improve photocatalytic properties:

- A two-step anodization method was developed, in which the obtained coatings were synthesized in an inorganic electrolyte with improved photoelectrochemical properties compared to a classic one-step anodization method.
- 2. The photoelectrochemical properties of anodic nanostructured TiO₂ (OCP, PCR, E_{Fb}, N_D) depend on the anodization parameters and the post-treatment heating atmosphere and temperature.
- 3. The obtainable crystalline structure depends on the parameters of the modified anodization, such as the voltage of the first step, the duration, and the total duration of anodization.
- 4. The activity of directly anodized NTs is insufficient for effective photocatalysis. Therefore, it is necessary to improve the coating activity.

A unique method of introducing additive material nanoparticles for obtaining composite coating has been developed to improve the photocatalytic activity. This *in situ* method allows for composite coatings of TiO₂ nanotubes, but its efficiency depends on the material and type of additives.

- 1. TiO₂ NTs synthesized in inorganic base electrolytes with WO₃ additive particles were tested and compared to the classical method of EPD.
- 2. The developed method provided better and more active photocatalytic coating than classical electrophoretic coating.
- 3. The coatings obtained in an inorganic base electrolyte showed a change in properties and a dependence of the crystalline structure on the introduced carbon additive material, uniquely promoting the brookite phase in anodic titania.
- The catalytic properties and parameters of the coatings obtained in an organic electrolyte depend on the type of additive material introduced.
 - a. The introduction of nitrogen-doped exfoliated multilayer graphene particles leads to a decrease in the E_{Fb} and N_D , whereas methylene blue degradation decreases. Indicating an overall reduction in catalytic

- performance that could be attributed to the collapse of the tubular structure.
- b. These particles (NC) Promote anatase formation.
- c. On the other hand introduction of CP material promotes brookite and rutile phase formation in anodic titania, which is a unique result.
- d. CP introduction increases photocatalytic properties of synthesized composite coating, maintaining tubular morphology.

The ability to enable brookite phase formation in anodic titania, as was observed in both inorganic and organic electrolytes, opens new possibilities for future investigating brookite in photocatalytic applications.

A summary of all investigated samples and parameter combinations is depicted in a mind map Fig. 46.

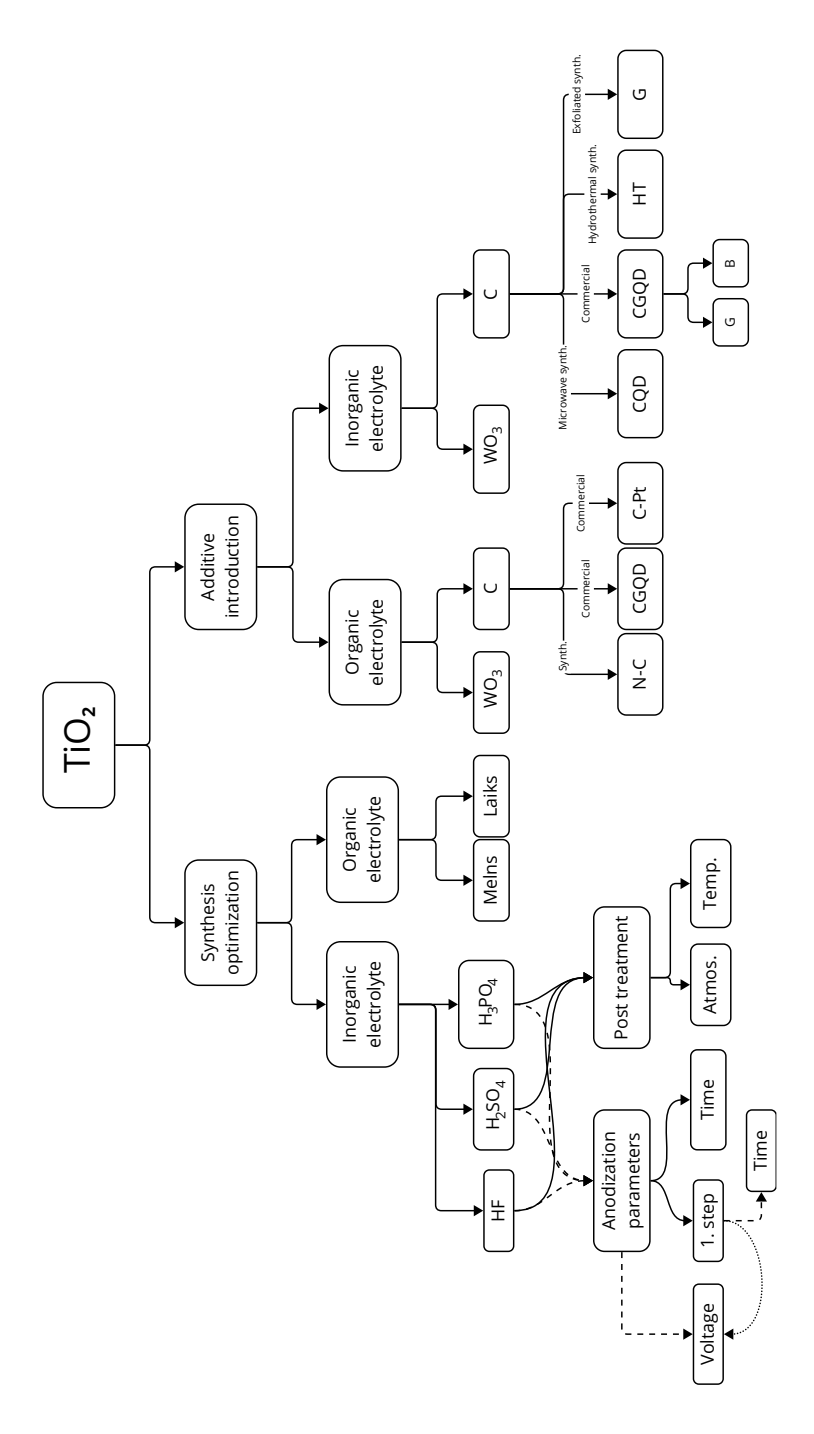


Fig 46. A schematic summary of the samples and parameters discussed in the work. Summary of modifications of the examined samples

5. ACKNOWLEDGEMENTS

First of all, I would like to thank the Institute of Solid State Physics, University of Latvia, for the opportunity to conduct research and develop this work, ensuring academic freedom and providing the opportunity to realize it. In addition, I greatly appreciate colleagues from ISSP UL and RTU TFI for conversations, help, clarification, training, and other kind of help in the technical use of equipment and methods and general education and improvement of professionalism.

Secondly, thanks to the students I have supervised in scientific, practical, and academic works for their diligence and questions, which helped me understand the processes and interpret the obtained data. Especially Raitis Sika and Roberts Palmbahs, who asked many questions regarding methods and processes as well as provided their opinion, which allowed us the development materials and methods.

Thirdly, I would like to express my greatest gratitude to my supervisor, Jānis Kleperis, for his great patience, academic freedom, leadership, and continuous, unwavering support in the processes of this work and my academic upbringing. As well as to Līga Grīnberga for constructive criticism and raising questions, language correction, and general support.

Fourth, I express my gratitude to my family for the greatest inspiration and support throughout this endeavor.

5.1. Projects and funding

Parts of the thesis research have been funded by the following projects:

- Preparation and study of anodic TiO₂ nanotubes doped with graphene quantum dots for photocatalytic CO₂ reduction. Scientific Research Project for Students and Young Researchers Nr. SJZ/2018/9 realized at the Institute of Solid State Physics, University of Latvia.
- Investigation of CO₂ decomposition and optimization of graphene exfoliation process. European Union's Horizon 2020 research and innovation programme under grant agreement No 768789 (CO₂EXIDE project).
- The authors gratefully acknowledge financial support from the Latvian Council of Science, Project LZP FLPP No. LZP-2018/1-0194
- This work has been supported by the European Social Fund within the Project No 8.2.2.0/18/A/017 "Development of the academic personnel of Riga Technical University in the strategic fields of specialization".
- Latvian Council of Science (project "Smart materials, photonics, technology and engineering ecosystem, project No. VPP-EM-FOTONIKA-2022/1-0001)

5.2. Participation in scientific projects and programs

- Latvian Council of Science (project "Smart materials, photonics, technology and engineering ecosystem, project No. VPP-EM-FOTONIKA-2022/1-0001) as researcher.
- 2. INNOvative catalyst and its regeneration for clean HYdrogen Production via methane Pyrolysis" (INNOHYPPY), 1.06.2023–30.04.2026, ISSP 185 kEUR as researcher (PI)
- 3. NATO Industry Advisory Group (NIAG) SG 284 on Military Implications of Novel Materials and Manufacturing Technologies 2022, as an expert.
- 4. Aluminum in circle economy from waste through hydrogen energy to Alumina (AliCE-WHy), 1.05.21–30.04.2024, The project is co-financed by the financial instrument of the European Economic Area 2014.–2021., participation as researcher and project manager (manager and factual PI), https://eegrants.lv/
- 5. CO-based Electrosynthesis of ethylene oXIDE CO₂EXIDE, 2018–2021, H2020, as researcher
- Trends, challenges and solutions of Latvian gas infrastructure development (LAGAS), Agreement No: VPP-EM-INFRA-2018/1-0003, Duration: 2019–2021, as researcher.
- Ar grafēna kvantu punktiem leģētu anodisko TiO₂ nanocaurulīšu iegūšana un izpēte fotokatalītiskai CO₂ reducēšanai. Nr. SJZ/2018/9 realized at the Institute of Solid State Physics, University of Latvia, 2018–2019
- 8. Research of optical, electrical and gas sensing properties of nanocarbon based polymer nanomaterials to be applied for harvesting and storage of renewable energy 2017, as assistant
- Centre of Excellence in Advanced Material Research and Technology (CAMART²), ISSP 32MEUR, participation is partial in various packages working as researcher and working with industry https://www.camart2.eu/ en/about/
- Nanostructured Nitrogenated Carbon Materials as Promoters in Energy Harvesting and Storage Technologies (2018–2021) NN-CARMA, FLPP, as research assistant
- 11. Synthesis and studies on controlled porosity composite thin layers and systems for energy storage and conversion applications Nr.666/2014 (2014–2017), FLPP, as engineer
- 12. Nanostructured materials for solid-state hydrogen storage (2011–2015), as engineer
- 13. Multifunctional Materials and composites, photonics and nanotechnology (IMIS) (2014–2017), as engineer

6. LIST OF USED LITERATURE

- [1] Kumar, R., Rashid, J., & Barakat, M. A. Zero valent Ag deposited TiO₂ for the efficient photocatalysis of methylene blue under UV-C light irradiation *Colloids and Interface Science Communications* (2015), 5, 1–4.
- [2] Bhowmick, G. D., Noori, M. T., Das, I., Neethu, B., Ghangrekar, M. M., & Mitra, A. Bismuth doped TiO₂ as an excellent photocathode catalyst to enhance the performance of microbial fuel cell *International Journal of Hydrogen Energy* (2018), 43(15), 7501–7510.
- [3] Paulose, M., Mor, G. K., Varghese, O. K., Shankar, K., & Grimes, C. A. Visible light photoelectrochemical and water-photoelectrolysis properties of titania nanotube arrays *Journal of Photochemistry and Photobiology A: Chemistry* (2006), *178*(1), 8–15.
- [4] Shaislamov, U., Kim, H., Yang, J. M., & Yang, B. L. CuO/ZnO/TiO₂ photocathodes for a self-sustaining photocell: Efficient solar energy conversion without external bias and under visible light *International Journal of Hydrogen Energy* (2020), 45(11), 6148–6158.
- [5] Madej, E., La Mantia, F., Mei, B., Klink, S., Muhler, M., Schuhmann, W., & Ventosa, E. Reliable benchmark material for anatase TiO₂ in Li-ion batteries: On the role of dehydration of commercial TiO₂ Journal of Power Sources (2014), 266, 155–161.
- [6] Dumitru, A., & Scott, K. Anode Materials for Microbial Fuel Cells In *Microbial Electrochemical and Fuel Cells: Fundamentals and Applications* (2016) (pp. 117–152). Elsevier Inc.
- [7] Ying, X., Shen, D., Wang, M., Feng, H., Gu, Y., & Chen, W. Titanium dioxide thin film-modified stainless steel mesh for enhanced current-generation in microbial fuel cells *Chemical Engineering Journal* (2018), 333, 260–267.
- [8] Wierzbicka, E., Schultz, T., Syrek, K., Sulka, G. D., Koch, N., & Pinna, N. Ultrastable self-standing Au nanowires/TiO₂ nanoporous membrane system for highperformance photoelectrochemical water splitting cells *Materials Horizons* (2022), 9(11), 2797–2808.
- [9] Xie, S., Zhang, Q., Liu, G., & Wang, Y. Photocatalytic and photoelectrocatalytic reduction of CO₂ using heterogeneous catalysts with controlled nanostructures *Chemical Communications* (2016), 52(1), 35–59.
- [10] Hasan, H., Hasan, M., Nahar, S., Kadhum, A., & Zain, M. Advances in Photocatalytic CO₂ Reduction with Water: A Review *Materials* (2017), 10(6), 629.
- [11] Batzill, M., Morales, E. H., & Diebold, U. Surface studies of nitrogen implanted ${\rm TiO_2}$ Chemical Physics (2007), 339(1–3), 36–43.
- [12] Ohya, Y., Saiki, H., Tanaka, T., & Takahashi, Y. Microstructure of TiO₂ and ZnO Films Fabricated by the Sol-Gel Method *Journal of the American Ceramic Society* (1996), 79(4), 825–830.
- [13] Krysa, J., Lee, K., Pausova, S., Kment, S., Hubicka, Z., Ctvrtlik, R., & Schmuki, P. Self-organized transparent 1D TiO₂ nanotubular photoelectrodes grown by anodization of sputtered and evaporated Ti layers: A comparative photoelectrochemical study *Chemical Engineering Journal* (2017), 308, 745–753.

- [14] Varnagiris, S., Medvids, A., Lelis, M., Milcius, D., & Antuzevics, A. Black carbon-doped TiO₂ films: Synthesis, characterization and photocatalysis *Journal of Photochemistry and Photobiology A: Chemistry* (2019), 382, 111941.
- [15] Oja, I., Mere, A., Krunks, M., Solterbeck, C.-H., & Es-Souni, M. Properties of TiO₂ Films Prepared by the Spray Pyrolysis Method Solid State Phenomena (2004), 99, 259–264.
- [16] Zimbone, M., Cacciato, G., Buccheri, M. A., Sanz, R., Piluso, N., Reitano, R., ... Privitera, V. Photocatalytical activity of amorphous hydrogenated TiO₂ obtained by pulsed laser ablation in liquid *Materials Science in Semiconductor Processing* (2016), 42, 28–31.
- [17] Zou, Y., Tan, X., Yu, T., Li, Y., Shang, Q., & Wang, W. Synthesis and photocatalytic activity of chrysanthemum-like brookite TiO₂ nanostructures *Materials Letters* (2014), 132, 182–185.
- [18] Sayes, C. M., Wahi, R., Kurian, P. A., Liu, Y., West, J. L., Ausman, K. D., ... Colvin, V. L. Correlating nanoscale titania structure with toxicity: A cytotoxicity and inflammatory response study with human dermal fibroblasts and human lung epithelial cells *Toxicological Sciences* (2006), 92(1), 174–185.
- [19] Shi, H., Magaye, R., Castranova, V., & Zhao, J. Titanium dioxide nanoparticles: A review of current toxicological data *Particle and Fibre Toxicology* (2013), *10*(1), 15.
- [20] Khan, Z., Shahwar, D., Yunus Ansari, M. K., & Chandel, R. Toxicity assessment of anatase (TiO₂) nanoparticles: A pilot study on stress response alterations and DNA damage studies in Lens culinaris Medik *Heliyon* (2019), 5(7), e02069.
- [21] Macák, J. M., Tsuchiya, H., & Schmuki, P. High-aspect-ratio TiO₂ nanotubes by anodization of titanium *Angewandte Chemie International Edition* (2005), 44(14), 2100–2102.
- [22] Lee, K., Mazare, A., & Schmuki, P. One-Dimensional Titanium Dioxide Nanomaterials: Nanotubes *Chemical Reviews* (2014), 114(19), 9385–9454.
- [23] Roy, P., Berger, S., Schmuki, P., & Schmuki, P. TiO 2 Nanotubes: Synthesis and Applications *Angew. Chem. Int. Ed* (2011), 50(13), 2904–2939.
- [24] Padiyan, D. P., & Raja, D. H. Synthesis of Various Generations Titania Nanotube Arrays by Electrochemical Anodization for $\rm H_2$ Production *Energy Procedia* (2012), 22, 88–100.
- [25] David, T. M., Dev, P. R., Wilson, P., Sagayaraj, P., & Mathews, T. A critical review on the variations in anodization parameters toward microstructural formation of TiO₂ nanotubes *Electrochemical Science Advances* (2022, August 1). John Wiley & Sons, Ltd.
- [26] Mor, G.K., Varghese, O. K., Paulose, M., Mukherjee, N., & Grimes, C. A. Fabrication of tapered, conical-shaped titania nanotubes *Journal of Materials Research* (2003), 18(11), 2588–2593.
- [27] Grimes, C. A., & Mor, G. K. TiO₂ Nanotube Arrays (2009). Boston, MA: Springer US.
- [28] Li, Y., Ma, Q., Han, J., Ji, L., Wang, J., Chen, J., & Wang, Y. Controllable preparation, growth mechanism and the properties research of TiO₂ nanotube arrays *Applied Surface Science* (2014), 297, 103–108.
- [29] Regonini, D., Groff, A., Sorarù, G. D., & Clemens, F. J. Photoelectrochemical study of anodized TiO₂ Nanotubes prepared using low and high H₂O contents *Electrochimica Acta* (2015), 186, 101–111.

- [30] Bauer, S., Kleber, S., & Schmuki, P. TiO₂ nanotubes: Tailoring the geometry in H₃PO₄/HF electrolytes *Electrochemistry Communications* (2006), 8(8), 1321–1325.
- [31] Mollavali, M., Falamaki, C., & Rohani, S. Preparation of multiple-doped ${\rm TiO_2}$ nanotube arrays with nitrogen, carbon and nickel with enhanced visible light photoelectrochemical activity via single-step anodization *International Journal of Hydrogen Energy* (2015), 40(36), 12239–12252.
- [32] Gaikwad, P. N., Wandre, T. M., Garadkar, K. M., Hankare, P. P., Jagannath, & Sasikala, R. Improvement of photocatalytic activity of TiO₂-WO₃ nanocomposite by the anionically substituted N and S Colloids and Surfaces A: Physicochemical and Engineering Aspects (2016), 506, 804–811.
- [33] Sellers, M. C. K., & Seebauer, E. G. Measurement method for carrier concentration in TiO₂ via the Mott-Schottky approach *Thin Solid Films* (2011), 519(7), 2103–2110.
- [34] He, Z., Xiao, J., Xia, F., Kajiyoshi, K., Samart, C., & Zhang, H. Enhanced solar water-splitting performance of TiO₂ nanotube arrays by annealing and quenching *Applied Surface Science* (2014), 313, 633−639.
- [35] Casu, A., Lamberti, A., Stassi, S., & Falqui, A. Crystallization of TiO₂ nanotubes by in situ heating TEM *Nanomaterials* (2018), 8(1).
- [36] Beranek, R. (Photo)electrochemical methods for the determination of the band edge positions of TiO₂-based nanomaterials Advances in Physical Chemistry (2011), 2011, 80–83.
- [37] Luttrell, T., Halpegamage, S., Tao, J., Kramer, A., Sutter, E., & Batzill, M. Why is anatase a better photocatalyst than rutile? Model studies on epitaxial TiO₂ films *Scientific Reports* (2015), 4(1), 4043.
- [38] Hoffmann, M. R., Martin, S. T., Choi, W., & Bahnemann, D. W. Environmental Applications of Semiconductor Photocatalysis *Chemical Reviews* (1995), 95(1), 69–96.
- [39] Sajjad, A. K. L., Shamaila, S., Tian, B., Chen, F., & Zhang, J. One step activation of WO_x/TiO₂ nanocomposites with enhanced photocatalytic activity *Applied Catalysis B: Environmental* (2009), 91(1–2), 397–405.
- [40] Singh, S. A., & Madras, G. Photocatalytic degradation with combustion synthesized WO₃ and WO₃TiO₂ mixed oxides under UV and visible light *Separation and Purification Technology* (2013), 105, 79–89.
- [41] Min, S., Hou, J., Lei, Y., Ma, X., & Lu, G. Facile one-step hydrothermal synthesis toward strongly coupled TiO₂/graphene quantum dots photocatalysts for efficient hydrogen evolution *Applied Surface Science* (2017), 396, 1375–1382.
- [42] Xie, H., Hou, C., Wang, H., Zhang, Q., & Li, Y. S, N Co-Doped Graphene Quantum Dot/TiO₂ Composites for Efficient Photocatalytic Hydrogen Generation Nanoscale Research Letters (2017), 12.
- [43] Gupta, B. K., Kedawat, G., Agrawal, Y., Kumar, P., Dwivedi, J., & Dhawan, S. K. A novel strategy to enhance ultraviolet light driven photocatalysis from graphene quantum dots infilled TiO₂ nanotube arrays RSC Advances (2015), 5(14), 10623– 10631.
- [44] Yu, L., Wang, Z., Shi, L., Yuan, S., Zhao, Y., Fang, J., & Deng, W. Photoelectrocatalytic performance of TiO₂ nanoparticles incorporated TiO₂ nanotube arrays *Applied Catalysis B: Environmental* (2012), 113–114, 318–325.
- [45] Porto, S. P. S., Fleury, P. A., & Damen, T. C. Raman Spectra of TiO₂, MgF₂, ZnF₂, FeF₂, and MnF₂ *Physical Review* (1967), *154*(2), 522–526.

- [46] Balachandran, U., & Eror, N. G. Raman spectra of titanium dioxide *Journal of Solid State Chemistry* (1982), 42(3), 276–282.
- [47] Regonini, Domenico Anodised TiO₂ Nanotubes: Synthesis, Growth Mechanism and Thermal Stability (2008). University of Bath.
- [48] Hardcastle, F. D. Raman Spectroscopy of Titania (TiO₂) Nanotubular Water-Splitting Catalysts *Journal of the Arkansas Academy of Science* (2011), 65.
- [49] Mor, Gopal K., Varghese, O. K., Paulose, M., Shankar, K., & Grimes, C. a. A review on highly ordered, vertically oriented TiO₂ nanotube arrays: Fabrication, material properties, and solar energy applications Solar Energy Materials and Solar Cells (2006), 90(14), 2011–2075.
- [50] Anandan, S., Sivasankar, T., & Lana-Villarreal, T. Synthesis of TiO_2/WO_3 nanoparticles via sonochemical approach for the photocatalytic degradation of methylene blue under visible light illumination *Ultrasonics Sonochemistry* (2014), 21(6), 1964–1968.
- [51] Fang, J., Bi, X., Si, D., Jiang, Z., & Huang, W. Spectroscopic studies of interfacial structures of CeO₂-TiO₂ mixed oxides *Applied Surface Science* (2007), 253(22), 8952–8961.
- [52] Ghobadi, A., Ulusoy, T. G., Garifullin, R., Guler, M. O., & Okyay, A. K. A heterojunction design of single layer hole tunneling ZnO passivation wrapping around TiO₂ nanowires for superior photocatalytic performance *Scientific Reports* (2016), 6(February), 30587.
- [53] Regonini, D., Bowen, C. R. R., Jaroenworaluck, A., & Stevens, R. A review of growth mechanism, structure and crystallinity of anodized TiO_2 nanotubes *Materials Science and Engineering R: Reports* (2013), 74(12), 377–406.
- [54] Regonini, D., Satka, A., Jaroenworaluck, A., Allsopp, D. W. E., Bowen, C. R., & Stevens, R. Factors influencing surface morphology of anodized TiO₂ nanotubes *Electrochimica Acta* (2012), 74, 244–253.
- [55] Baran, E., & Yazıcı, B. Fabrication of TiO₂-NTs and TiO₂-NTs covered honeycomb lattice and investigation of carrier densities in I–/I3– electrolyte by electrochemical impedance spectroscopy *Applied Surface Science* (2015), 357, 2206–2216.
- [56] Tauc, J., Grigorovici, R., & Vancu, A. Optical Properties and Electronic Structure of Amorphous Germanium *Physica Status Solidi (B)* (1966), 15(2), 627–637.
- [57] Tauc, J. Optical properties and electronic structure of amorphous Ge and Si *Materials Research Bulletin* (1968), 3(1), 37-46.
- [58] Stenzel, O. Solid State Optics In *The Physics of Thin Film Optical Spectra* (2005) (pp. 199–228). Berlin/Heidelberg: Springer-Verlag.
- [59] Olins, R., Lesnicenoks, P., Kleperis, J., Knoks, A., & Lukosevics, I. Electrochemical exfoliation-streamline method for synthesis of nitrogen doped graphene *Chemija* (2021), 32(1), 9–16.
- [60] Erol, M., Dikici, T., Toparli, M., & Celik, E. The effect of anodization parameters on the formation of nanoporous TiO2 layers and their photocatalytic activities *Journal of Alloys and Compounds* (2014), 604, 66–72.
- [61] Wang, X., Zhang, S., & Sun, L. A Two-step anodization to grow high-aspect-ratio TiO₂ nanotubes *Thin Solid Films* (2011), 519(15), 4694–4698.

- [62] Nishanthi, S. T., Sundarakannan, B., Subramanian, E., & Pathinettam Padiyan, D. Enhancement in hydrogen generation using bamboo like TiO₂ nanotubes fabricated by a modified two-step anodization technique *Renewable Energy* (2015), 77, 300–307.
- [63] Yang, Y., Wang, X., & Li, L. Synthesis and growth mechanism of graded TiO₂ nanotube arrays by two-step anodization *Materials Science and Engineering: B* (2008), 149(1), 58-62.
- [64] Macak, J. M., Albu, S., Kim, D. H., Paramasivam, I., Aldabergerova, S., & Schmuki, P. Multilayer TiO₂ -Nanotube Formation by Two-Step Anodization *Electrochemical* and Solid-State Letters (2007), 10(7), K28.
- [65] John, A., Naduvath, J., Mallick, S., Shripathi, T., Thankamoniamma, M., & Philip, R. R. A novel cost effective fabrication technique for highly preferential oriented TiO2 nanotubes *Nanoscale* (2015), 7(48), 20386–20390.
- [66] Ding, D., Zhou, B., Fu, W., Lv, P., Yao, H., Liu, L., ... Yang, H. Varied crystalline orientation of anatase TiO₂ nanotubes from [101] to [001] promoted by TiF62– ions and their enhanced photoelectrochemical performance *Journal of Materials Science* (2018), 53(5), 3332–3340.
- [67] Acevedo-Peña, P., González, F., González, G., & González, I. The effect of anatase crystal orientation on the photoelectrochemical performance of anodic TiO₂ nanotubes *Physical Chemistry Chemical Physics* (2014), 16(47), 26213–26220.
- [68] Albu, S. P., Tsuchiya, H., Fujimoto, S., & Schmuki, P. TiO₂ nanotubes Annealing effects on detailed morphology and structure In *European Journal of Inorganic Chemistry* (2010) (Vol. 2010, pp. 4351–4356). John Wiley & Sons, Ltd.
- [69] Hu, Y., Pan, Y., Wang, Z., Lin, T., Gao, Y., Luo, B., ... Wang, L. Lattice distortion induced internal electric field in TiO2 photoelectrode for efficient charge separation and transfer *Nature Communications* (2020), 11(1), 1–10.
- [70] Kim, M., Bae, C., Kim, H., Yoo, H., Montero Moreno, J. M., Jung, H. S., ... Shin, H. Confined crystallization of anatase TiO₂ nanotubes and their implications on transport properties *Journal of Materials Chemistry A* (2013), 1(45), 14080–14088.
- [71] Cui, Z. H., Wu, F., & Jiang, H. First-principles study of relative stability of rutile and anatase TiO₂ using the random phase approximation *Physical Chemistry Chemical Physics* (2016), *18*(43), 29914–29922.
- [72] Seremak, W., Baszczuk, A., Jasiorski, M., Gibas, A., & Winnicki, M. Correction to: Photocatalytic Activity Enhancement of Low-pressure Cold-Sprayed TiO₂ Coatings Induced by Long-term Water Vapor Exposure (Journal of Thermal Spray Technology, (2021), 30, 7, (1827–1836), 10.1007/s11666-021-01244-5) Journal of Thermal Spray Technology (2022, October 1). Springer.
- [73] Yoo, J. E., & Schmuki, P. Critical Factors in the Anodic Formation of Extremely Ordered Titania Nanocavities *Journal of The Electrochemical Society* (2019), *166*(11), C3389–C3398.
- [74] Gemelli, E., & Camargo, N. H. A. Oxidation kinetics of commercially pure titanium *Matéria (Rio de Janeiro)* (2007), 12(3), 525–531.
- [75] Ting, C. C., Chen, S. Y., & Liu, D. M. Structural evolution and optical properties of TiO₂ thin films prepared by thermal oxidation of sputtered Ti films *Journal of Applied Physics* (2000), 88(8), 4628–4633.
- [76] Besra, L., & Liu, M. A review on fundamentals and applications of electrophoretic deposition (EPD) *Progress in Materials Science* (2007), 52(1), 1–61.

- [77] Zhao, Y., Hoivik, N., & Wang, K. Study of TiO₂ Nanotube Formation Mechanisms by Simulation on Electric Domain *The Electrochemical Society Study* (2014), 61(36), 9–13.
- [78] Knoks, A., Kleperis, J., Bajars, G., Grinberga, L., & Bogdanova, O. WO₃ as Additive for Efficient Photocatalyst Binary System TiO₂/WO₃ Latvian Journal of Physics and Technical Sciences (2021), 58(6), 24–34.
- [79] Patterson, A. L. The Scherrer Formula for X-Ray Particle Size Determination *Physical Review* (1939), 56(10), 978–982.
- [80] Knoks, Ainars, Grinberga, L., & Kleperis, J. Novel Anodic TiO₂ Synthesis Method with Embedded Graphene Quantum Dots for Improved Photocatalytic Activity Coatings 2024, Vol. 14, Page 1407 (2024), 14(11), 1407.
- [81] Ceballos-Chuc, M. C., Ramos-Castillo, C. M., Alvarado-Gil, J. J., Oskam, G., & Rodríguez-Gattorno, G. Influence of brookite impurities on the raman spectrum of TiO₂ anatase nanocrystals *Journal of Physical Chemistry C* (2018), 122(34), 19921–19930.
- [82] Kandiel, T. A., Robben, L., Alkaim, A., & Bahnemann, D. Brookite versus anatase TiO₂ photocatalysts: Phase transformations and photocatalytic activities In Photochemical and Photobiological Sciences (2013) (Vol. 12, pp. 602–609). Royal Society of Chemistry.
- [83] Chou, P.-W., Wang, Y.-S., Lin, C.-C., Chen, Y.-J., Cheng, C.-L., & Wong, M.-S. Effect of carbon and oxygen on phase transformation of titania films during annealing *Surface and Coatings Technology* (2009), 204(6), 834–839.
- [84] Santara, B., Giri, P. K., Imakita, K., & Fujii, M. Microscopic origin of lattice contraction and expansion in undoped rutile TiO₂ nanostructures *Journal of Physics D: Applied Physics* (2014), 47(21), 215302.
- [85] Rajender, G., Kumar, J., & Giri, P. K. Interfacial charge transfer in oxygen deficient TiO₂-graphene quantum dot hybrid and its influence on the enhanced visible light photocatalysis *Applied Catalysis B: Environmental* (2018), 224, 960–972.
- [86] Luan, N. H., & Chang, C. F. Efficient fabrication of robust and highly ordered free-standing TiO₂ nanotube layers *Materials Research Bulletin* (2022), *151*, 111829.
- [87] Taib, M. A. A., Alias, N., Jaafar, M., Razak, K. A., Tan, W. K., Shahbudin, I. P., ... Lockman, Z. Formation of grassy TiO₂ nanotube thin film by anodisation in peroxide electrolyte for Cr(VI) removal under ultraviolet radiation *Nanotechnology* (2020), 31(43), 435605.
- [88] Novoselov, K. S., Geim, A. K., Morozov, S. V., Jiang, D., Zhang, Y., Dubonos, S. V., ... Firsov, A. A. Electric field in atomically thin carbon films *Science* (2004), 306(5696), 666–669.
- [89] Knoks, Ainars, Sika, R., Olins, R., & Lesnicenoks, P. Investigation of carbon nanomaterial influence on photocatalytic properties of TiO₂ In Engineering for Rural Development (2021) (Vol. 20, pp. 1804–1813).